Medaka and zebrafish *contactin1* mutants as a model for understanding neural circuits for motor coordination

Miki Takeuchi[1], Chikako Inoue[1], Akiko Goshima[2], Yusuke Nagao[1], Koichi Shimizu[2], Hiroki Miyamoto[3], Takashi Shimizu[1,2], Hisashi Hashimoto[1,2], Shigenobu Yonemura[4], Atsuo Kawahara[5], Yutaka Hirata[3], Masayuki Yoshida[6], Masahiko Hibi[1,2,*]

[1]Laboratory of Organogenesis and Organ Function, Bioscience and Biotechnology Center, Nagoya University, Nagoya, Aichi 464-8601, Japan
[2]Division of Biological Science, Graduate School of Science, Nagoya University, Nagoya, Aichi 464-8602, Japan
[3]Department of Computer Science, Chubu University, 1200 Matsumoto, Kasugai, Aichi 485-8501, Japan
[4]RIKEN Center for Life Science Technologies, Kobe, Hyogo, Japan
[5]Laboratory for Developmental Biology, Center for Medical Education and Sciences, Graduate School of Medical Science, University of Yamanashi, Yamanashi 409-3898, Japan
[6]Graduate School of Biosphere Sciences, Hiroshima University, Kagamiyama 1-4-4, Higashihiroshima, Hiroshima 739-8528, Japan

Short title: Neural circuits in *cntn1*-mutant fish
Keywords: Contactin1, swimming behavior, medaka, zebrafish

*Correspondence: hibi@bio.nagoya-u.ac.jp
Laboratory of Organogenesis and Organ Function, Bioscience and Biotechnology Center, Nagoya University, Furo, Chikusa, Nagoya 464-8601, Tel: +81-52-789-5198, Fax: +81-52-789-5053

Abstract

A spontaneous medaka *ro* mutant shows abnormal wobbling and rolling swimming behaviors. By positional cloning, we mapped the *ro* locus to a region containing the gene encoding Contactin1b (Cntn1b), which is an immunoglobulin (Ig)-superfamily domain-containing membrane-anchored protein. The *ro* mutant had a deletion in the *cntn1b* gene that introduced a premature stop codon. Furthermore, *cntn1b* mutants generated by the CRISPR/Cas9 system and trans-heterozygotes of the CRISPR mutant allele and *ro* had abnormal swimming behavior, indicating that the *cntn1b* gene was responsible for the *ro*-mutant phenotype. We also established zebrafish *cntn1a* and *cntn1b* mutants by transcription activator-like effector nucleases (TALENs). Zebrafish *cntn1b* but not *cntn1a* mutants showed abnormal swimming behaviors similar to those in the *ro* mutant, suggesting that Cntn1b plays a conserved role in the formation or function of the neural circuits that control swimming in teleosts. Although *Cntn1*-deficient mice have abnormal cerebellar neural circuitry, there was no apparent histological abnormality in the cerebellum of medaka or zebrafish *cntn1b* mutants. The medaka *cntn1b* mutants had defective optokinetic response (OKR) adaptation and abnormal rheotaxis (body positioning relative to water flow). Medaka and zebrafish *cntn1b* mutants are effective models for studying the neural circuits involved in motor learning and motor coordination.

Introduction

Swimming is a complex behavior in fish that involves neural circuits in the sensory and motor control systems (Arnold 1974). During swimming, the central nervous system (CNS) receives sensory inputs from the lateral line (water flow), vestibular system (balance), eyes (visual information), and other CNS regions, and coordinately controls the fin muscles to swim, just as land animals coordinate their limb muscles to walk or run. Although the sensory and motor systems involved in swimming behavior are relatively well understood, how the neural circuits integrate inputs and control the motor system for smooth swimming remains to be elucidated. One strategy for investigating this issue is to examine mutant fish with abnormal swimming behavior.

Medaka (*Oryzias latipes*) and zebrafish (*Danio rerio*) are useful models for investigating neural-circuit development and function, since their anatomy, development, and behavior are relatively well understood and many mutants have been isolated. In the late twentieth century, Hideo Tomita of Nagoya University isolated 94 naturally occurring medaka mutant strains called the Tomita collection (Tomita 1975, 1990, 1992). The medaka *ro* mutant, which is a Tomita-collection mutant, rolls abnormally when swimming in high temperatures as an adult. Fish with the *ro* mutation, which is autosomal recessive, are fertile despite their abnormal swimming behavior. Although the *ro* locus has been suggested to be involved in the development or function of the neural circuits that control swimming, its molecular nature has not been identified. In this study, we identified the *ro* locus as the *contactin1b* (*cntn1b*) gene.

Like other members of the Contactin (Cntn) family, Cntn1 (previously known

as F11 in chickens and F3 in mice) is a membrane-anchored molecule with six Ig-superfamily domains, four fibronectin type III (FN) domains, and a GPI (glycosyl phosphatidyl inositol) anchor (Ranscht 1988; Brummendorf *et al.* 1989; Gennarini *et al.* 1989; Shimoda & Watanabe 2009). In mice, Cntn1 is expressed in differentiated neurons in various regions of the CNS, including granule cells, Golgi cells, and Purkinje cells in the cerebellum; pyramidal and granule neurons in the hippocampus; olfactory nerve fibers, mitral cells, and synaptic glomeruli in the olfactory sensory system (Faivre-Sarrailh *et al.* 1992; Virgintino *et al.* 1999); in specialized domains of myelinated fibers called the nodes and paranodes of Ranvier (Peles & Salzer 2000; Girault & Peles 2002; Poliak & Peles 2003; Salzer 2003); and at neuromuscular junctions (Compton *et al.* 2008). Whereas mammals have only one *Cntn1* gene, two paralogous genes *cntn1a* and *cntn1b* encode Cntn1 in teleosts (Haenisch *et al.* 2005; Schweitzer *et al.* 2007). In early-stage larval zebrafish, *cntn1a* and *cntn1b* are differentially expressed in the CNS and peripheral nervous system, including the retina, midbrain, hindbrain, spinal cord, and trigeminal/lateral-line ganglia (Haenisch *et al.* 2005).

Cntn1-deficient mice have a severe ataxic phenotype and defects in granule-cell axon guidance and in dendritic projections from granule and Golgi cells (Berglund *et al.* 1999). A *Cntn1* deficiency also disrupts the paranode in myelinated nerve fibers and degrades nerve condition (Boyle *et al.* 2001), and impairs long-term depression (LTD) in the hippocampus (Murai *et al.* 2002). In humans, *CNTN1* mutations are linked to a form of lethal congenital myopathy (Compton *et al.* 2008),

although there is no apparent myopathy in *Cntn1*-deficient mice (Davisson *et al.* 2011). These data indicate that Cntn1 is important in myelination, synaptic plasticity, and cerebellar neural-circuit formation in mammals. However, because *Cntn1* mouse mutants show early postnatal lethality (at 2–3 weeks) (Berglund *et al.* 1999; Davisson *et al.* 2011), it is difficult to study Cntn1's roles in the formation and function of neural circuits that are involved in later animal behaviors such as locomotion (walking, running, and swimming).

For this study, we generated zebrafish *cntn1a* and *cntn1b* mutants as well as medaka *cntn1b* (*ro*) mutants, and found that Cntn1b was required for proper swimming in both medaka and zebrafish. We further demonstrated that Cntn1b was prerequisite for OKR adaptation and the body positioning in rheotaxis. Our data indicate that *cntn1*-mutant medaka and zebrafish are suitable models for studying the neural circuits responsible for motor learning and motor coordination in vertebrates.

Results

Positional cloning of the *ro* locus

Hideo Tomita described the *ro*-mutant medaka as exhibiting rolling behavior at high temperature (Tomita 1990, 1992). We confirmed that an existing line of adult *ro*-mutant fish showed rolling (upside-down) behavior soon after their water was heated to 30 °C (Movie S1). The fish also wobbled when swimming, reflecting abnormal balancing, even at the normal breeding temperature (26 °C) (Movies S2). This abnormal behavior

was not seen in hatchlings, but was observed beginning around one month post-fertilization (mpf). The phenotype became more severe during the juvenile stage (1–2 mpf) and was evident in all adult *ro* mutants (3 mpf onward). Despite these abnormal behaviors, *ro* mutants are fertile, and the strains have been maintained by incrossing *ro*-mutant adults. For positional cloning, the *ro* mutants were crossed with wild-type HNI-I or Kaga strains (from the Northern medaka), which have a different genetic background from the *ro* mutant (Hyodo-Taguchi 1996). The F1 fish behaved normally, but 22.2% of the F2 adult fish produced by incrossing the F1 generation (271/1200 from the *ro*/HNI-I cross and 242/1112 from the *ro*/Kaga cross) displayed the rolling behavior at 30 °C. There was no bias in the expressivity of the phenotypes between males and females. Our data confirmed that *ro* is an autosomal recessive mutation and that it is not strictly temperature-sensitive. Compared to zebrafish ear mutants, which have defective vestibular function and begin to show rolling behavior in the larval stages (Granato *et al.* 1996; Whitfield *et al.* 1996), the *ro* mutants had a late-onset rolling phenotype. Bulked segregant analysis of the phenotypic F2 genomes mapped the *ro* locus to a region of chromosome 23 that contains a few genes (Fig. 1A). Among these genes, we considered *cntn1b* to be a good candidate, because its orthologue is expressed in the zebrafish and mouse CNS, and mouse *Cntn1* is involved in the formation and function of neural circuits (Faivre-Sarrailh *et al.* 1992; Granato *et al.* 1996; Whitfield *et al.* 1996; Virgintino *et al.* 1999). We then isolated and compared the sequences of *cntn1b* cDNA from wild-type and *ro*-mutant brains. The *ro*-mutant *cntn1b* had a 23-bp deletion on the 3′ side of the region coding the sixth Ig domain,

which generates a premature stop codon and truncates the FN domains and the GPI-anchor domain (Fig. 1E). The 23-bp deletion was located in exon 15 of the *cntn1b* gene in the *ro*-mutant genome (Fig. 1B, C). In the *ro*-mutant brain, the expression of *cntn1b* but not its neighboring genes was reduced (Fig. 1D), suggesting that the *cntn1b* transcripts in the *ro* mutant underwent nonsense-mediated RNA decay. These data suggested that *cntn1b* is the gene responsible for the *ro* mutant.

The *ro* locus encodes Cntn1b

Although the mutation in *cntn1b* was correlated with the abnormal swimming phenotypes in the positional-cloning analysis, there could have been another causative gene in the vicinity of the *cntn1b* locus. Thus, to confirm that *cntn1b* was the gene responsible for the *ro* mutation, we generated *cntn1b* mutants using a CRISPR/Cas9 method. We designed guide RNA (gRNA) for targets in exons 3 and 6 of medaka *cntn1b* (Fig. 1F), and injected Cas9 RNA and the gRNA into F0 fish. As adults, many of the F0 fish showed rolling behavior similar to that of *ro*-mutant fish, while no abnormal swimming behaviors were observed in F0 fish injected with Cas9 RNA and a control gRNA (for *nrcam*). The F0 fish were crossed with wild-type medaka to establish three F1 *cntn1b* mutant lines: one exon-3 mutant ($cntn1b^{E3+35}$) and two exon-6 mutants ($cntn1b^{E6-22}$ and $cntn1b^{E6-4}$) (Fig. 1G; Fig. S1). All F2–5 adult fish homozygous for the $cntn1b^{E3+35}$, $cntn1b^{E6-22}$, or $cntn1b^{E6-4}$ mutations showed the same wobbling or rolling behaviors as the *ro* mutant (Table 1), but all of the heterozygotes swam normally. We then crossed the *ro*-mutant fish and $cntn1b^{E3+35/+}$ fish, and found that all of the

trans-heterozygote mutant fish having both the *ro* mutation (23-bp deletion) and the *cntn1b*$^{E3+35}$ allele (*cntn*$^{ro/E3+35}$) had the same abnormal swimming behaviors, indicating that the CRISPR mutation of *cntn1b* did not complement the *ro* mutation (Table 1). Taken together, our data showed that *cntn1b* is the causative gene for the *ro* mutation.

Expression of *cntn1a* and *cntn1b* in the CNS

We next examined the *cntn1b* and *cntn1a* expression in medaka by RT-PCR, which revealed that both *cntn1a* and *cntn1b* are expressed zygotically (Fig. 2A), and that *cntn1a* expression begins at the early gastrula period (stage 14) while *cntn1b* expression commences at the segmentation (or neurula) period (stage 23) (Fig. 2A). Whole-mount *in situ* hybridization showed that *cntn1a* is expressed in the tectum, the trigeminal ganglia, the anterior and posterior lateral-line ganglia, and a subset of neurons in the spinal cord (stage 34, Fig. 2B–G), while *cntn1b* is expressed in the retina, the nuclei of the medial longitudinal fasciculus, the trigeminal ganglia, the anterior and posterior lateral-line ganglia, a cluster of hindbrain neurons (likely reticulospinal neurons), and spinal-cord neurons at the pharyngula period (stage 34, Fig. 2H–M). These expression patterns were similar to those reported for zebrafish *cntn1a* and *cntn1b* (Haenisch *et al.* 2005). In the adult medaka brain, *cntn1a* and *cntn1b* transcripts were found in overlapping and distinct domains of the telencephalon, diencephalon (including the hypothalamus), optic tectum, and hindbrain (including the cerebellum) (Fig. 3). Compared to *cntn1a*, *cntn1b* was expressed in more cells in the adult brain. We examined the aldolase C, fructose-bisphosphate, a (*aldoca*) expression, which marks

Purkinje cells, and the GABA A receptor, alpha 6b (*gabra6b*) expression, which marks granule cells (Bahn *et al.* 1996; Jones *et al.* 1996; Volkmann *et al.* 2008; Tanabe *et al.* 2010), and found that *cntn1a* and *cntn1b* are expressed in Purkinje cells in the cerebellum and in differentiated granule cells in the cerebellum and the torus longitudinalis of the optic tectum (Fig. 3A′, B′, C, D). The cerebellar expression of *cntn1a/1b* in medaka was also consistent with that of mouse *Cntn1* in the cerebellum (Ranscht 1988; Gennarini *et al.* 1989; Virgintino *et al.* 1999), suggesting that *cntn1* expression in the cerebellum is essentially conserved between teleosts and mammals. RT-PCR confirmed the expression of *cntn1b* in eye and brain, but did not detect its expression in heart, testis, intestine, or liver in the adult medaka fish (Fig. S2).

Medaka *ro* (*cntn1b*)-mutant fish have no gross abnormalities in the CNS structure or cerebellum

To investigate how the *cntn1b* deficiency causes abnormal swimming, we compared the CNS of *ro*-mutant and wild-type adults. Nissl staining showed that the medaka *ro*-mutant fish exhibited no gross abnormalities in the cell composition in the telencephalon, diencephalon, mesencephalon, or hindbrain (Fig. 4A, C). Since a *Cntn1* deficiency in mice leads to cerebellar neural-circuit abnormalities that are linked to ataxia, which is abnormal motor coordination (Berglund *et al.* 1999), we examined the cerebellar structure of the *ro* mutant. The lobular structure, consisting of the valvula cerebelli, corpus cerebelli, lobus caudalis, eminentia granularis, and the layer structures, consisting of the molecular layer and granule-cell layer (GCL), of the cerebellum

appeared normal in *ro* mutants (Fig. 4B, D). Immunostaining for carbonic anhydrase VIII (Ca8) and vesicular glutamate transporter 1 (Vglut1, also known as Slc17a7a), which mark Purkinje cells and granule-cell axons, respectively (Bae *et al.* 2009), showed that the Purkinje-cell somata and dendrites and granule-cell axons were largely unaffected in the *ro*-mutant cerebellum (Fig. 4E–J). These data indicated that Cntn1b is not essential for the development of lobular and layer structures, or for the differentiation or neurite formation of Purkinje and granule cells.

Conserved role of Cntn1b in medaka and zebrafish swimming

Although the medaka *ro* mutant is a useful model, zebrafish studies can provide additional or alternative information about the roles of Cntn-family proteins in CNS development and function, since many tools are available for zebrafish research. We generated zebrafish with *cntn1a* and *cntn1b* mutations using TALENs designed for two targets in the putative exon 5 of *cntn1a*, and for targets in exons 5 and 9 of *cntn1b* (Fig. 5A). We injected the TALEN RNA, or gRNA with Cas9 RNA, into zebrafish embryos at the one-cell stage. In the founder generations, we successfully isolated two mutant alleles each for the zebrafish *cntn1a* and *cntn1b* genes ($cntn1a^{nub8}$, $cntn1a^{nub9}$, $cntn1b^{nub10}$, and $cntn1b^{nub11}$; Fig. 5B; Fig. S3). All of the mutant alleles were likely to be null alleles, since they had an insertion or a deletion (indel) mutation that caused a frame shift in the open reading frame (ORF) and introduced a premature stop codon that generated a truncated protein lacking the FN and GPI domains. Homozygotes of the *cntn1a* and *cntn1b* mutants were able to grow to adulthood. The homozygous *cntn1a*

mutants (*cntn1a*^{nub8} and *cntn1a*^{nub9}) swam normally, but the homozygous *cntn1b* adult mutants (*cntn1b*^{nub10} and *cntn1b*^{nub11}) exhibited abnormal wobbling and rolling behaviors at the normal breeding temperature (28 °C) (Table 2, Movie S3), as observed in the *ro*-mutant medaka. These abnormal swimming behaviors affected the feeding behavior, and most of the homozygous *cntn1b* mutants became thin and died earlier than wild-type siblings or heterozygotes carrying the same mutation. These data suggested that the role of Cntn1b in swimming-related neural circuits is conserved between medaka and zebrafish.

Cntn1a and Cntn1b are not essential for forming the cerebellum in zebrafish

We next examined the cerebellum in zebrafish *cntn1* mutants by immunostaining for parvalbumin7 (Pvalb7), which marks Purkinje cells, and for Vglut1, which marks granule-cell axons. Zebrafish *cntn1a* and *cntn1b* single-mutant fish had no apparent abnormalities in the Purkinje cells or granule-cell axons in the cerebellum at the early larval stage of 5 days post-fertilization (dpf) or in adulthood (Fig. 5C–Q, Fig. 6A–I). Furthermore, there were no apparent abnormalities in the Purkinje or granule cells in *cntn1a; cntn1b* double-mutant larvae at 5 dpf (Fig. 6J–L). These data indicated that Cntn1a and Cntn1b are not essential for the development of the cerebellum, although it is unclear whether they are required for the function of cerebellar neural circuits.

Cntn1b is required for learning from ONI training

To determine which CNS functions were affected in the *cntn1b*-deficient fish, we

investigated oculomotor control (Fig. 7) and rheotaxis (Fig. 8), which are related to swimming behavior, in the medaka *ro*-mutant adult fish. We first examined the optokinetic response (OKR) using horizontal oculomotor neural integrator (ONI) training, which has been applied extensively in goldfish (Major *et al.* 2004a; Major *et al.* 2004b; Debowy & Baker 2011). The ONI located in the posterior hindbrain is involved in the persistent firing of oculomotor neurons to generate a tonic eye-position command for gaze holding. Continuous visual stimulation improves the OKR, in which the ONI controls oculomotor neurons more efficiently to follow visual cues (Kheradmand & Zee 2011). Cerebellar neural circuits are involved in ONI-mediated OKR adaptation in various vertebrate species, including fish (Marsh & Baker 1997; Debowy & Baker 2011; reviewed in Kheradmand & Zee 2011). ONI instability training uses rotating visual stimuli to increase the eye velocity in proportion to eye position after each scanning saccade (Fig. 7A, B). Eye velocity gradually increased with prolonged exposure to the visual stimuli (Fig. 7B; magenta line indicates the slope of eye-position drift) in wild-type medaka, as in goldfish (Major *et al.* 2004a), but there was little improvement in the *ro*-mutant eye velocity (Fig. 7C). These data suggested that in medaka, Cntn1b is required for OKR adaptation, which represents ONI learning performance.

Cntn1b is required for rheotaxis

We next analyzed rheotaxis in the *ro*-mutant fish (Fig. 8). When swimming against a current, medaka fish control their fin movement to maintain their body position. We

placed wild-type medaka and *ro* mutants in a swim-mill chamber, increased the speed of the water flow stepwise to 1, 2, 3, and 4 body lengths (BL)/s, and tracked the head position during swimming. We resolved position changes on the y-axis (perpendicular to the swimming direction) into low (1–4 Hz) and high (4–20 Hz) frequencies, which roughly represent body displacement and head yawing, respectively, and determined the strength of the positional change in each component as a root mean square (RMS) (Fig. 8, S4). Medaka fish swim to maintain their body position in rheotaxis. When the water flow was slow (1 or 2 BL/s), there was little body displacement or head yawing (low RMS). When the water flow increased, the head displacement and head yawing (higher RMS) increased in both wild-type and *ro*-mutant medaka (Fig. S4). The strength of both body displacement and head yawing differed between wild-type medaka and *ro* mutants (Fig. S4), and in fast-flow conditions (4 BL/s), the body displacement and head swings were significantly larger in the *ro* mutants (Fig. 8B). These data indicated that Cntn1b is required for proper rheotaxis in medaka.

Discussion

Here, we identified *cntn1b* as the gene responsible for the *ro* mutant's abnormal swimming behavior. The *ro*-mutant phenotype was more severe at 30 °C than at 26 °C, and included rolling behavior at the higher temperature. However, the *ro* mutation of *cntn1b* introduces a premature stop codon that causes nonsense-mediated RNA decay (Fig. 1). Thus, the *ro* mutation is likely to be a null allele, which does not explain its

temperature-sensitive phenotype. Given that *ro*-mutant fish began rolling immediately after their water temperature was raised to 30 °C, high-temperature stimulation probably does not induce a conformational change of the mutant Cntn1b protein, but instead overloads the sensory system so that the fish cannot control its swimming behavior in the absence of Cntn1b.

In *Cntn1*-deficient mice, cerebellar neural circuits develop abnormally, the paranodes in peripheral myelinated nerves are disrupted, LTD is impaired in the hippocampus, and the mice show early postnatal lethality (Berglund *et al.* 1999; Boyle *et al.* 2001; Murai *et al.* 2002; Davisson *et al.* 2011), indicating that Cntn1 plays multiple roles in neural-circuit development in the vertebrate CNS. However, medaka and zebrafish *cntn1b* mutants could survive into adulthood. Medaka *cntn1b*-mutant *ro* fish are fertile and can be maintained as homozygotes over many generations by incrossing. Thus, the effect of the *cntn1b* deficiency is milder in medaka and zebrafish than in mice. Zebrafish and medaka underwent teleost-specific whole-genome duplication (Amores *et al.* 1998; Postlethwait *et al.* 1998; Kasahara *et al.* 2007), and thus have two *cntn1* genes. In both zebrafish and medaka, *cntn1a* and *cntn1b* are expressed in overlapping domains of the CNS (Fig. 2, 3) (Haenisch *et al.* 2005), suggesting that *cntn1a* and *cntn1b* play redundant roles in CNS development and function. Thus, the *cntn1b*-deficiency phenotypes in medaka and zebrafish reflect a partial loss of Cntn1, which may correspond to hypomorphic mutations or a conditional *Cntn1* knockout in mammals. Careful examination of the medaka and zebrafish *cntn1b* mutants may reveal subtle anomalies in paranode structures in the myelinated peripheral

nerves or in synaptic plasticity in some regions of the CNS, as in *Cntn1*-deficient mice, although those anomalies do not affect the survival of the mutant fish. Mutations in the human *CNTN1* gene are linked to congenital myopathy (Compton *et al.* 2008), whereas *Cntn1*-deficient mice do not have myopathy phenotypes (Davisson *et al.* 2011). We observed that some aged populations of *cntn1b*-mutant medaka and zebrafish adults (over one year old) were misshapen, but it is not clear whether this was associated with any type of myopathy. Phenotypic analyses of these medaka and zebrafish mutants may contribute to our understanding of Cntn1's common and species-specific roles in development.

Cntn1-deficient mice have misoriented granule-cell axons (parallel fibers) and defective dendritic projections from Golgi and granule cells (Berglund *et al.* 1999). However, there were no gross abnormalities in the lobular or layer structures of the cerebellum in the medaka and zebrafish *cntn1b* mutants (Fig. 4, 5). Immunostaining for Vglut1 revealed that the orientation of granule-cell axons was not affected in zebrafish larvae homozygous for the *cntn1a*, *cntn1b*, or *cntn1a; cntn1b* mutations (Fig. 6). Cntn1 may suppress the proliferation of granule-cell progenitors in mice (Xenaki *et al.* 2011). However, the number of Neurod1^{+} differentiating and mature granule cells in zebrafish *cntn1a, cntn1b,* or *cntn1a; cntn1b* mutant larvae did not differ significantly from that in wild-type larvae (Fig. S5). Furthermore, we could not find apparent differences in the cerebellar structure of adult wild-type versus *ro*-mutant medaka when examined by electron microscopy. These histological data suggest that the role of Cntn1 in cerebellar development differs between mammals and teleosts, although the mild phenotypes in

medaka and zebrafish might also be explained by a partial loss of Cntn1 function in *cntn1b* mutants, or by a rescue by other *cntn*-family genes in *cntn1a; cntn1b* mutants. Multiple *cntn*-family genes are expressed during cerebellar development (Stoeckli 2010), and the expression profile and functions of each *cntn* gene (and its paralogues) may vary by species. The compensation of *cntn1* deficiency by other *cntn* genes might contribute to the milder phenotypes in medaka and zebrafish *cntn1* mutants, and this type of compensation might also differ between mammals and teleosts.

Although *cntn1b*-mutant medaka and zebrafish had no gross cerebellar abnormalities, the *cntn1b* deficiency might still affect cerebellar neural-circuit functions. The cerebellum plays important roles in oculomotor control (Kheradmand & Zee 2011), and cerebellar lesions in mammals or cerebellar degeneration in human diseases leads to abnormal oculomotor control such as defective OKR, vestibular-ocular reflex, and gaze holding (Leech *et al.* 1977; Estanol *et al.* 1979; Zee *et al.* 1981; Hotson 1982; Eckmiller & Westheimer 1983; Godaux & Vanderkelen 1984). The horizontal ONI, which is located in the posterior hindbrain in goldfish and contains multiple types of neurons (Pastor *et al.* 1994; Aksay *et al.* 2007), maintains the eye position in gaze holding by a sustained discharge of oculomotor neurons. The vestibulocerebellum, which is the caudal-most part of the cerebellum in mammals and corresponds to the lobus caudalis cerebelli and eminentia granularis in the teleost cerebellum, plays an important role in ONI learning: it modulates the horizontal ONI's activity via a positive feedback loop to improve eye movement (Kheradmand & Zee 2011). OKR adaptation, which represents the ONI learning performance, was impaired in *cntn1b*-mutant medaka fish (Fig. 7),

suggesting that Cntn1b may be required for the function of cerebellar neural circuits. *Cntn1*-deficient mice have abnormal cerebellar neural circuits and ataxia (Berglund *et al.* 1999). The abnormal swimming behavior of *cntn1b*-mutant medaka and zebrafish might be comparable to the ataxic gait seen in *Cntn1*-deficient mice, since both involve the coordinated motor control of appendage muscles. Our data suggest that small changes in synapses and other microstructures in the cerebellar neural circuits of *cntn1b*-mutant medaka and zebrafish might cause abnormalities in oculomotor response and swimming. Electrophysiological analysis, which is feasible for studying cerebellar functions (Hsieh *et al.* 2014; Sengupta & Thirumalai 2015; Scalise *et al.* 2016), will reveal whether and how cerebellar neural circuits are affected in the mutants.

We found that medaka *cntn1b*-mutant fish have abnormal rheotaxis (Fig. 8). In fish, rheotaxis involves detecting the water flow and visual, tactile, lateral-line, and likely vestibular stimuli (Arnold 1974). The sensory information is integrated in the CNS to coordinate and control the fin muscles. The abnormal rheotaxis in *cntn1b* mutants might be linked to sensory-system abnormalities. However, the initial OKR (before training) was not affected in the c*ntn1b* mutants (Fig. 7), suggesting that these mutants received visual inputs normally. Zebrafish vestibular mutants begin the abnormal rolling behavior at an early larval stage (Granato *et al.* 1996; Whitfield *et al.* 1996). In contrast, the medaka *cntn1b* mutant larvae had normal swimming behavior and touch responses, suggesting that their motor control and development of vestibular and tactile responses was normal. Although the possibility cannot be excluded that the sensory (e.g. vestibular) and motor systems in these mutants degenerate during the

juvenile and adult stages, their abnormal rheotaxis and swimming behaviors are likely to be related to abnormal development of the neural circuits that integrate sensory information to elicit motor coordination. Zebrafish and medaka develop optokinetic learning ability and vestibuloocular behavior during their first month (Beck *et al.* 2004), indicating that the neural circuits that control motor coordination are established during the larval period. Cntn1b may be required for this process. Cntn1b is expressed not only in cerebellar neurons, but also in premotor neurons, such as in the nuclei of medial longitudinal fasciculus and in reticulospinal neurons (Fig. 2), which control fin muscles by regulating motoneurons in the spinal cord (Uematsu *et al.* 2007; Kohashi & Oda 2008; Kimura *et al.* 2013; Thiele *et al.* 2014). Cntn1b may be involved at several points in the formation of the neural circuits that control motor coordination. Thus, medaka and zebrafish *cntn1b* mutants provide a useful model for investigating the neural circuits that control motor learning and motor coordination.

Experimental procedures

Ethics statement

The animal work in this study was approved by the Nagoya University Animal Experiment Committee (approval numbers 2014020503, 2015022304, and 2016022203) and was conducted in accordance with Regulations on Animal Experiments in Nagoya University.

Medaka and zebrafish strains and husbandry

For medaka fish, this study used the Nagoya and orange-red (OR) strains as wild-type *Oryzias latipes*. We also used the *ro*-mutant medaka, isolated by Hideo Tomita (Tomita 1990, 1992) and maintained at the National Institute of Radiological Sciences, and used the HNI-I and Kaga strains (Hyodo-Taguchi 1996) for crossing in the genetic mapping study. For zebrafish, we used wild-type zebrafish with an Oregon AB genetic background. The medaka and zebrafish were maintained in tanks with a water-circulating system (Meitosuien) at 26 °C (medaka) or 28 °C (zebrafish) under a 14-h light/10-h dark cycle at the Bioscience and Biotechnology Center, Nagoya University.

Positional cloning

F1 *ro* and wild-type HNI-I or Kaga hybrids were crossed to produce F2 offspring, which were raised to adulthood and maintained at 30 °C. F2 fish displaying abnormal wobbling or rolling during swimming (n=316) were selected and examined by bulked segregant analysis using the M-marker system (Kimura *et al.* 2004; Kimura & Naruse 2010). For further recombination analysis, polymorphic markers were isolated by referring to the medaka genome database (Ensemble Medaka: http://asia.ensembl.org/Oryzias_latipes/Info/Index). A 23-bp deletion in exon 15 of the *cntn1b* gene was detected by PCR using the primers 5′-CAGGCTAACAAGTGGGTCAC-3′ and 5′- AATGGGGCTATTATGCTCTG-3′. Detailed information about the markers used is shown in Table S1.

Reverse transcription (RT)-PCR

Total RNA was isolated from medaka embryos or hatchlings or from the adult brain, including the forebrain, midbrain, and hindbrain, using TRI Reagent (Molecular Research Center, Inc.) according to the manufacturer's protocol. One microgram of total RNA was used to generate cDNA in 20 µl of solution using ReverTra Ace (Toyobo). The cDNA was subjected to semi-quantitative PCR using KOD-Plus-Neo and the primers 5′- CGGGATCCGCCGGCGGCAGGACACCACC-3′ and 5′-CGGAATTCGGTGGAGGGGCATACTCAGAC-3′ for *slc25a3b*, 5′-CGGAATTCACGTTGCCCGAGCTGCCATC-3′ and 5′-CCGCTCGAGACACCACGGGGACACGGCGC-3′ for *ldhba*, and 5′-CGGAATTCGTCTAAACTCAACGTGCTGTC-3′ and 5′-TTGGATTTCCAAGAGCAAAG -3′ for *cntn1b*. We detected *ef1α* as previously described (Kinoshita *et al.* 2000).

Generation of medaka *cntn1b* mutants by CRISPR/Cas9

CRISPR/Cas9 targets were selected in exons 3 and 6 of the medaka *cntn1b* gene using the web software ZiFiT Targeter 4.2 (http://zifit.partners.org/ZiFiT/) (Hwang *et al.* 2013; Mali *et al.* 2013). To generate gRNA, the oligonucleotides 5′-TAGGTGGATGTGGTCTACACTG-3′ and 5′-AAACCAGTGTAGACCACATCCA-3′ or 5′-TAGGGGAACTTGTACATTTCCA-3′ and 5′-AAACTGGAAATGTACAAGTTCC-3′ were annealed and subcloned to pT7-gRNA (Jao *et al.* 2013) to introduce mutations in exons 3 and 6. As a control, we also designed

gRNAs for *nrcam*, which encodes an Ig-superfamily protein and is located in the same chromosome as *cntn1b*. The oligonucleotides 5′-TAGGGAAGGCCGAGGCCTACGA-3′ and 5′-AAACTCGTAGGCCTCGGCCTTC-3′ (for exon 4 of *nrcam*) or 5′-TAGGGAGCAAGGATCAGGTTCT-3′ and 5′-AAACAGAACCTGATCCTTGCTC-3′ (for exon 10 of *nrcam*) were annealed and subcloned to pT7-gRNA. The gRNAs were synthesized from *BamH*I-digested pT7-gRNA plasmids with T7 RNA polymerase (Promega). The Cas9 RNA was synthesized from pCS2+hSpCas9 (Ansai & Kinoshita 2014), which contains the human codon–optimized *S. pyogenes* Cas9 gene (Cong *et al.* 2013), in the presence of m′G(5′)ppp(5′)G RNA Cap Structure Analog (NEB). A solution containing 6.6-23 ng/μl gRNA and 266 ng/μl Cas9 RNA was injected into medaka embryos at the one-cell stage. To detect indel mutations, the target regions were amplified by PCR using the primers described below and were subjected to heteroduplex mobility analysis (HMA) (Ota *et al.* 2013). The mutations were confirmed by sequencing after subcloning of the target regions amplified from the mutant genome into pGEM-T Easy (Promega) or pTAC-2 (BioDynamics Laboratory Inc.). The PCR primers used to detect the exon 3 mutation of *cntn1b* (*cntn1b*$^{E3+35}$) were 5′-GTCCCTCTTTTTGAGAAATGAG-3′ and 5′-TTTCTGTCGCTCACCTGTAG-3′; the primers to detect the exon 6 mutation of *cntn1b* (*cntn1b*$^{E6-22}$ and *cntn1b*$^{E6-4}$) were 5′-GTTCCCCGTGTTCCTGCATACG-3′ and 5′-AATTTCCGGCATCCTGAGCT-3′. Since *cntn1b*$^{E3+35}$ and *cntn1b*$^{E6-22}$ have relatively long insertions and deletions, the PCR products from these mutant alleles were analyzed

on 3% agarose gels. PCR products from *cntn1b*$^{E6\text{-}4}$ were analyzed on 20% acrylamide gels.

TALEN generation of zebrafish *cntn1a* and *cntn1b* mutants

The TALENs for zebrafish *cntn1a/cntn1b* were designed with the web software TALEN Targeter 2.0 (https://tale-nt.cac.cornell.edu/node/add/talen) (Cermak *et al.* 2011) to introduce mutations in the putative exon 5 (two different regions) in *cntn1a* and exon 5/9 in *cntn1b*. The first TALENs for *cntn1a* contained the following repeat variable diresidues (RVDs): NN HD NG NN NI NG HD NI NN HD NG HD NI HD HD and NN NG NI NN NG NG NG HD HD HD NN HD NI NG, and target 5′-GCTGATCAGCTCACC-3′ and 5′-GTAGTTTCCCGCAT-3′. The second TALENS for *cntn1a* contained the following RVDs: NN NN HD HD NI NN HD NI NI HD HD NI NN NG NI HD and NN NG NI HD NG HD NG NN NN HD NG HD NG HD HD, and target 5′-GGCCAGCAACCAGTAC-3′ and 5′-GTACTCTGGCTCTCC-3′. The TALENs for exon 5 of *cntn1b* contained the following RVDs: NN NN NG HD NI NG NG NI HD NI NI NI HD HD and NI HD NI NG NI NG NG NG NG HD HD NI NN HD NI NG, and target 5′- GGTCATTACAAACC-3′ and 5′-ACATATTTTCCAGCAT-3′. The TALENs for exon 9 of *cntn1b* contained the following RVDs: NN NN NI NN HD NG NG NG NI HD NG NG HD NI HD HD NG and NN HD HD HD NG HD NN NG HD HD NG HD NI NG, and target 5′-GGAGCTTTACTTCACCT-3′ and 5′-GCCCTCGTCCTCAT-3′. The TALEN cDNAs were constructed as previously described (Sakuma *et al.* 2013) and subcloned into

pCS2pTAL3DD and pCS2pTALRR (Dahlem *et al.* 2012). Capped RNAs were synthesized from *Not*I-digested TALEN expression plasmids by SP6 RNA polymerase (Promega) in the presence of m′G(5′)ppp(5′)G RNA Cap Structure Analog. One nanoliter of solution containing a pair of TALEN RNAs (0.4 μg/μl each) was injected into zebrafish embryos at the one-cell stage. Indel mutations in the target region were detected with HMA and high-resolution melting analysis (HRMA) as previously described (Dahlem *et al.* 2012; Ota *et al.* 2013). We used the following PCR primers: for the first exon-5 mutant of *cntn1a* (*cntn1a*^{nub8}), 5′-GGGCGGTGATCCTCACTACAGT-3′ and 5′GTTGCTGGCCACACAGGTGT-3′; for the second exon-5 mutant of *cntn1a* (*cntn1a*^{nub9}), 5′-CTGTGTGGCCAGCAACCAGT-3′ and 5′-GAACTGCACTCTGGCTCTCC-3′; for the exon-5 mutant of *cntn1b* (*cntn1b*^{nub10}), 5′-ATGAGCACTTCAGCCTGGTTGG-3′ and 5′-CCGTACACGTTCTTGGCCAC-3′; and for the exon-9 mutant of *cntn1b* (*cntn1b*^{nub11}), 5′-CCCGCCAAACTATGAAGTCAGC-3′ and 5′-TCCCTTTCACATTGAGCGTC-3′.

In situ hybridization

In situ hybridization was performed as previously described (Bae *et al.* 2009; Nagao *et al.* 2010; Nagao *et al.* 2014). A digoxigenin (DIG)-labeled riboprobe was made from a cloned template in pGEM-T Easy or pBluescript II SK+ (Agilent) using SP6, T3, or T7 RNA polymerase after restriction-enzyme digestion. To make the templates, cDNA fragments of medaka *cntn1a*, *cntn1b*, *aldoca*, and *gabra6b* were amplified with the PCR

primers listed in Table S2. For whole-mount *in situ* hybridization, fixed embryos were treated with Proteinase K (10 μg/ml) in phosphate-buffered saline (PBS) for 10 min at 30 °C before hybridization. For sections, the brain was removed from adult medaka or zebrafish and fixed overnight at 4 °C in 4% paraformaldehyde in PBS. The specimens were immersed in 20% sucrose solution overnight at 4 °C, frozen in OCT compound (Sakura Finetechnical), and sectioned at 12–14 μm on a cryostat. Hybridization was performed at 65 °C overnight. Signals were detected with alkaline-phosphatase conjugated with anti-DIG Fab fragments (Roche) using NBT/BCIP (Roche) as a chromogenic substrate. NBT/BCIP signals were acquired using an AioPlan-2 microscope and AxioCam CCD camera (Zeiss).

Immunohistochemistry

Anti-Ca8, anti-Pvalb7, anti-zebrafish-Vglut1, and anti-Neurod1 antibodies were as previously reported (Bae *et al.* 2009; Kani *et al.* 2010). The anti-Ca8 antibody cross-reacted with medaka Ca8. The anti-medaka-Vglut1 antibody was generated by immunizing rabbits with the synthetic peptide CPGHNSYMHEREKEKELS (the underlined C was added to link the peptide covalently with keyhole-limpet hemocyanin). For immunostaining, we used anti-Ca8 (1:100, mouse hybridoma supernatant), anti-Pvalb7 (1:1000, mouse ascites), anti-zebrafish-Vglut1 (1:1000, rabbit purified antibody), anti-medaka-Vglut1 (1:500, rabbit serum), and anti-Neurod1 (1:500, mouse ascites). Larvae and cryosections were immunostained as described previously (Bae *et al.* 2009). Alexa Fluor 488, Alexa Fluor 555 goat anti-mouse, and goat anti-rabbit IgG

(H+L, Molecular Probes, Thermo Fisher Scientific) were used singly or in combination as secondary antibodies. Fluorescence images were obtained with an LSM700 confocal laser-scanning microscope (Zeiss). The images were constructed from Z-stack sections using the 3D-projection program associated with the microscope (Zen, Zeiss). The figures were constructed using Adobe Photoshop and Adobe Illustrator. Brightness and contrast adjustments were applied equally to all digital images in each figure.

ONI training for medaka

The experimental setup consisted of a PVC cylindrical water tank (104-mm diameter, 100-mm depth), an infrared camera (DMK21BF04, Imaging Source), an optokinetic visual stimulator (OKS), and a personal computer (PC) (Fig. 7). The water tank was connected to a reservoir tank with aeration, filtering, and temperature control to maintain the water quality and keep the water at 20 °C. The fish was restrained at the center of the water tank with a head holder fixed to a metal pin that was glued onto the frontal bones of the fish. The camera was placed atop the water tank to acquire magnified images of the animal's right eye for eye-movement measurements. The OKS consisted of a planetarium device that projected random dots generated by a high-luminance white-light-emitting diode (LED, NSPWR70CS, Nichia) and a servo motor (CSK545AP, Oriental Motor Inc.) driven by the PC via a data acquisition device (DAQ, NI USB-6009, National Instruments) to rotate the planetarium. The OKS was placed under the water tank in a transparent acrylic dome attached to the bottom of the water tank, so that the random dots from the planetarium were sharply projected and

rotated on the tank wall. The PC acquired eye images from the camera via an IEEE1394 port, and the rotation angle of the eye (eye position) in real time (60 frames/sec) was detected with custom-made software developed on the LabVIEW Vision Toolkit (National Instruments). The software also generated motor commands that were sent to the servomotor via the DAQ according to the measured eye positions to induce ONI motor learning in the fish. The ONI instability training was previously described (Major *et al.* 2004a; Debowy & Baker 2011). Briefly, immediately after each saccade made spontaneously by the fish, an OKS pattern (random dots in the current setup) was rotated in the direction away from the null position of the eye. In the present experiment, the null eye position was determined as the center of the movable range of the eye. The OKS rotation velocity was set in proportion to the eye position relative to the null position. The visual stimulation induced OKR, which caused eye-position drifts away from the null position after each saccade, as exemplified in the inset of Fig. 7B. In offline analysis using MATLAB (Mathworks), the ONI training effect was measured by the steepness of the eye-position drifts after saccades during instability training. A linear function was fitted to each eye-position drift by the least-squares method, and the estimated slope of the regression line was evaluated as the steepness of the drift. To evaluate learning curves, the estimated slopes were averaged in every 100-second window that contained more than 50 saccades.

Rheotaxis analysis

After measuring the body length (BL) of an adult medaka fish, the fish was place in a

swim-mill chamber (10 cm in the y axis, which is parallel to the flow direction, and 2 cm in the x axis). The water flow in the chamber was set at a velocity of 1, 2, 3, or 4 BL/s, and swimming behavior was recorded by a video camera (DMK 23U021, Imaging Source) set up over the chamber. The head position of the fish was tracked in the recorded video with Tracker ver. 4.87 (http://physlets.org/tracker/) and recorded as x/BL and y/BL. A stereotaxic period was defined as a time period in which the fish kept a stereotaxic position within 0.5 BL in both the x and y axes for 1 s and did not swim close to the chamber wall. Stereotaxic periods longer than 7 s were selected for further analysis. The y-axis movements of the head position during the stereotaxic period were separated into low-frequency (1–4 Hz) and high-frequency (4–20 Hz) components, representing body displacement and head yawing, respectively, using LabChart (ADInstruments). The RMS value of each component was calculated and used for statistical analyses and to evaluate the stability of swimming against the water flow.

Statistics

Data were analyzed for statistical significance by Fisher's exact test, Welch's *t* test, and one-way or two-way repeated-measures ANOVA using GraphPad PRISM (ver. 5.01).

Acknowledgements

We thank Y. Ishikawa and K. Maruyama for providing the *ro*-mutant medaka, M. Kinoshita and F. Zhang for the hSpCas9 plasmid, T. Yamamoto and K. Hoshijima for the TALEN-related plasmids, A. Koga for assistance with statistical analysis, I. Hara

and Y. Kamei for technical assistance with the HRMA, Y. Tsukazaki and K. Kondoh for fish mating and care, and the members of the Hibi laboratory for helpful discussions.

References

Aksay, E., Olasagasti, I., Mensh, B.D., Baker, R., Goldman, M.S. & Tank, D.W. (2007) Functional dissection of circuitry in a neural integrator. *Nat Neurosci* **10**, 494-504.

Amores, A., Force, A., Yan, Y.L., Joly, L., Amemiya, C., Fritz, A., Ho, R.K., Langeland, J., Prince, V., Wang, Y.L., Westerfield, M., Ekker, M. & Postlethwait, J.H. (1998) Zebrafish hox clusters and vertebrate genome evolution. *Science* **282**, 1711-1714.

Ansai, S. & Kinoshita, M. (2014) Targeted mutagenesis using CRISPR/Cas system in medaka. *Biology Open* **3**, 362-371.

Arnold, G.P. (1974) Rheotropism in fishes. *Biological Reviews of the Cambridge Philosophical Society* **49**, 515-576.

Bae, Y.K., Kani, S., Shimizu, T., Tanabe, K., Nojima, H., Kimura, Y., Higashijima, S. & Hibi, M. (2009) Anatomy of zebrafish cerebellum and screen for mutations affecting its development. *Developmental Biology* **330**, 406-426.

Bahn, S., Harvey, R.J., Darlison, M.G. & Wisden, W. (1996) Conservation of gamma-aminobutyric acid type A receptor alpha 6 subunit gene expression in cerebellar granule cells. *J Neurochem* **66**, 1810-1818.

Beck, J.C., Gilland, E., Tank, D.W. & Baker, R. (2004) Quantifying the ontogeny of optokinetic and vestibuloocular behaviors in zebrafish, medaka, and goldfish. *J Neurophysiol* **92**, 3546-3561.

Berglund, E.O., Murai, K.K., Fredette, B., Sekerkova, G., Marturano, B., Weber, L., Mugnaini, E. & Ranscht, B. (1999) Ataxia and abnormal cerebellar microorganization in mice with ablated contactin gene expression. *Neuron* **24**, 739-750.

Boyle, M.E., Berglund, E.O., Murai, K.K., Weber, L., Peles, E. & Ranscht, B. (2001) Contactin orchestrates assembly of the septate-like junctions at the paranode in myelinated peripheral nerve. *Neuron* **30**, 385-397.

Brummendorf, T., Wolff, J.M., Frank, R. & Rathjen, F.G. (1989) Neural cell recognition molecule F11: homology with fibronectin type III and immunoglobulin type C domains. *Neuron* **2**, 1351-1361.

Cermak, T., Doyle, E.L., Christian, M., Wang, L., Zhang, Y., Schmidt, C., Baller, J.A., Somia, N.V., Bogdanove, A.J. & Voytas, D.F. (2011) Efficient design and assembly of

custom TALEN and other TAL effector-based constructs for DNA targeting. *Nucleic Acids Research* **39**, e82.

Compton, A.G., Albrecht, D.E., Seto, J.T., Cooper, S.T., Ilkovski, B., Jones, K.J., Challis, D., Mowat, D., Ranscht, B., Bahlo, M., Froehner, S.C. & North, K.N. (2008) Mutations in contactin-1, a neural adhesion and neuromuscular junction protein, cause a familial form of lethal congenital myopathy. *American Journal of Human Genetics* **83**, 714-724.

Cong, L., Ran, F.A., Cox, D., Lin, S., Barretto, R., Habib, N., Hsu, P.D., Wu, X., Jiang, W., Marraffini, L.A. & Zhang, F. (2013) Multiplex genome engineering using CRISPR/Cas systems. *Science* **339**, 819-823.

Dahlem, T.J., Hoshijima, K., Jurynec, M.J., Gunther, D., Starker, C.G., Locke, A.S., Weis, A.M., Voytas, D.F. & Grunwald, D.J. (2012) Simple methods for generating and detecting locus-specific mutations induced with TALENs in the zebrafish genome. *PLoS Genetics* **8**, e1002861.

Davisson, M.T., Bronson, R.T., Tadenev, A.L., Motley, W.W., Krishnaswamy, A., Seburn, K.L. & Burgess, R.W. (2011) A spontaneous mutation in contactin 1 in the mouse. *PLoS One* **6**, e29538.

Debowy, O. & Baker, R. (2011) Encoding of eye position in the goldfish horizontal oculomotor neural integrator. *J Neurophysiol* **105**, 896-909.

Eckmiller, R. & Westheimer, G. (1983) Compensation of oculomotor deficits in monkeys with neonatal cerebellar ablations. *Exp Brain Res* **49**, 315-326.

Estanol, B., Romero, R. & Corvera, J. (1979) Effects of cerebellectomy on eye movements in man. *Arch Neurol* **36**, 281-284.

Faivre-Sarrailh, C., Gennarini, G., Goridis, C. & Rougon, G. (1992) F3/F11 cell surface molecule expression in the developing mouse cerebellum is polarized at synaptic sites and within granule cells. *The Journal of Neuroscience: the official journal of the Society for Neuroscience* **12**, 257-267.

Gennarini, G., Cibelli, G., Rougon, G., Mattei, M.G. & Goridis, C. (1989) The mouse neuronal cell surface protein F3: a phosphatidylinositol-anchored member of the immunoglobulin superfamily related to chicken contactin. *The Journal of Cell Biology* **109**, 775-788.

Girault, J.A. & Peles, E. (2002) Development of nodes of Ranvier. *Current Opinion in Neurobiology* **12**, 476-485.

Godaux, E. & Vanderkelen, B. (1984) Vestibulo-ocular reflex, optokinetic response and their interactions in the cerebellectomized cat. *J Physiol* **346**, 155-170.

Granato, M., van Eeden, F.J., Schach, U., Trowe, T., Brand, M., Furutani-Seiki, M., Haffter, P., Hammerschmidt, M., Heisenberg, C.P., Jiang, Y.J., Kane, D.A., Kelsh, R.N., Mullins, M.C., Odenthal, J. & Nusslein-Volhard, C. (1996) Genes controlling and mediating locomotion behavior of the zebrafish embryo and larva. *Development* **123**, 399-413.

Haenisch, C., Diekmann, H., Klinger, M., Gennarini, G., Kuwada, J.Y. & Stuermer, C.A. (2005) The neuronal growth and regeneration associated Cntn1 (F3/F11/Contactin) gene is duplicated in fish: expression during development and retinal axon regeneration. *Molecular and Cellular Neurosciences* **28**, 361-374.

Hotson, J.R. (1982) Cerebellar control of fixation eye movements. *Neurology* **32**, 31-36.

Hsieh, J.Y., Ulrich, B., Issa, F.A., Wan, J. & Papazian, D.M. (2014) Rapid development of Purkinje cell excitability, functional cerebellar circuit, and afferent sensory input to cerebellum in zebrafish. *Front Neural Circuits* **8**, 147.

Hwang, W.Y., Fu, Y., Reyon, D., Maeder, M.L., Tsai, S.Q., Sander, J.D., Peterson, R.T., Yeh, J.R. & Joung, J.K. (2013) Efficient genome editing in zebrafish using a CRISPR-Cas system. *Nature Biotechnology* **31**, 227-229.

Hyodo-Taguchi, Y. (1996) Inbred strains of the medaka, *Oryzias latipes*. *Fish Biol J MEDAKA* **8**, 11-14.

Jao, L.E., Wente, S.R. & Chen, W. (2013) Efficient multiplex biallelic zebrafish genome editing using a CRISPR nuclease system. *Proceedings of the National Academy of Sciences of the United States of America* **110**, 13904-13909.

Jones, A., Bahn, S., Grant, A.L., Kohler, M. & Wisden, W. (1996) Characterization of a cerebellar granule cell-specific gene encoding the gamma-aminobutyric acid type A receptor alpha 6 subunit. *J Neurochem* **67**, 907-916.

Kani, S., Bae, Y.K., Shimizu, T., Tanabe, K., Satou, C., Parsons, M.J., Scott, E., Higashijima, S. & Hibi, M. (2010) Proneural gene-linked neurogenesis in zebrafish cerebellum. *Dev Biol* **343**, 1-17.

Kasahara, M., Naruse, K., Sasaki, S. *et al.* (2007) The medaka draft genome and insights into vertebrate genome evolution. *Nature* **447**, 714-719.

Kheradmand, A. & Zee, D.S. (2011) Cerebellum and ocular motor control. *Front Neurol* **2**, 53.

Kimura, T., Jindo, T., Narita, T., Naruse, K., Kobayashi, D., Shin, I.T., Kitagawa, T., Sakaguchi, T., Mitani, H., Shima, A., Kohara, Y. & Takeda, H. (2004) Large-scale isolation of ESTs from medaka embryos and its application to medaka developmental genetics. *Mechanisms of Development* **121**, 915-932.

Kimura, T. & Naruse, K. (2010) M-marker 2009, a marker set for mapping medaka mutants using PCR length polymorphisms with an automated microchip gel electrophoresis system. *BioTechniques* **49**, 582-583.

Kimura, Y., Satou, C., Fujioka, S., Shoji, W., Umeda, K., Ishizuka, T., Yawo, H. & Higashijima, S. (2013) Hindbrain V2a neurons in the excitation of spinal locomotor circuits during zebrafish swimming. *Current Biology: CB* **23**, 843-849.

Kinoshita, M., Kani, S., Ozato, K. & Wakamatsu, Y. (2000) Activity of the medaka translation elongation factor 1alpha-A promoter examined using the GFP gene as a reporter. *Development, Growth & Differentiation* **42**, 469-478.

Kohashi, T. & Oda, Y. (2008) Initiation of Mauthner- or non-Mauthner-mediated fast escape evoked by different modes of sensory input. *The Journal Of Neuroscience: the official journal of the Society for Neuroscience* **28**, 10641-10653.

Leech, J., Gresty, M., Hess, K. & Rudge, P. (1977) Gaze failure, drifting eye movements, and centripetal nystagmus in cerebellar disease. *Br J Ophthalmol* **61**, 774-781.

Major, G., Baker, R., Aksay, E., Mensh, B., Seung, H.S. & Tank, D.W. (2004a) Plasticity and tuning by visual feedback of the stability of a neural integrator. *Proceedings of the National Academy of Sciences of the United States of America* **101**, 7739-7744.

Major, G., Baker, R., Aksay, E., Seung, H.S. & Tank, D.W. (2004b) Plasticity and tuning of the time course of analog persistent firing in a neural integrator. *Proceedings of the National Academy of Sciences of the United States of America* **101**, 7745-7750.

Mali, P., Yang, L., Esvelt, K.M., Aach, J., Guell, M., DiCarlo, J.E., Norville, J.E. & Church, G.M. (2013) RNA-guided human genome engineering via Cas9. *Science* **339**, 823-826.

Marsh, E. & Baker, R. (1997) Normal and adapted visuooculomotor reflexes in goldfish. *J Neurophysiol* **77**, 1099-1118.

Murai, K.K., Misner, D. & Ranscht, B. (2002) Contactin supports synaptic plasticity associated with hippocampal long-term depression but not potentiation. *Current Biology: CB* **12**, 181-190.

Nagao, Y., Cheng, J., Kamura, K., Seki, R., Maeda, A., Nihei, D., Koshida, S., Wakamatsu, Y., Fujimoto, T., Hibi, M. & Hashimoto, H. (2010) Dynein axonemal intermediate chain 2 is required for formation of the left-right body axis and kidney in medaka. *Developmental Biology* **347**, 53-61.

Nagao, Y., Suzuki, T., Shimizu, A. *et al.* (2014) Sox5 functions as a fate switch in medaka pigment cell development. *PLoS Genetics* **10**, e1004246.

Ota, S., Hisano, Y., Muraki, M., Hoshijima, K., Dahlem, T.J., Grunwald, D.J., Okada, Y. & Kawahara, A. (2013) Efficient identification of TALEN-mediated genome modifications using heteroduplex mobility assays. *Genes to Cells: Devoted to Molecular & Cellular Mechanisms* **18**, 450-458.

Pastor, A.M., De la Cruz, R.R. & Baker, R. (1994) Eye position and eye velocity integrators reside in separate brainstem nuclei. *Proceedings of the National Academy of Sciences of the United States of America* **91**, 807-811.

Peles, E. & Salzer, J.L. (2000) Molecular domains of myelinated axons. *Current Opinion in Neurobiology* **10**, 558-565.

Poliak, S. & Peles, E. (2003) The local differentiation of myelinated axons at nodes of Ranvier. *Nature reviews. Neuroscience* **4**, 968-980.

Postlethwait, J.H., Yan, Y.L., Gates, M.A. *et al.* (1998) Vertebrate genome evolution and the zebrafish gene map. *Nat Genet* **18**, 345-349.

Ranscht, B. (1988) Sequence of contactin, a 130-kD glycoprotein concentrated in areas of interneuronal contact, defines a new member of the immunoglobulin supergene family in the nervous system. *The Journal of Cell Biology* **107**, 1561-1573.

Sakuma, T., Hosoi, S., Woltjen, K., Suzuki, K., Kashiwagi, K., Wada, H., Ochiai, H., Miyamoto, T., Kawai, N., Sasakura, Y., Matsuura, S., Okada, Y., Kawahara, A., Hayashi, S. & Yamamoto, T. (2013) Efficient TALEN construction and evaluation methods for human cell and animal applications. *Genes to Cells: Devoted to Molecular & Cellular Mechanisms* **18**, 315-326.

Salzer, J.L. (2003) Polarized domains of myelinated axons. *Neuron* **40**, 297-318.

Scalise, K., Shimizu, T., Hibi, M. & Sawtell, N.B. (2016) Responses of cerebellar Purkinje cells during fictive optomotor behavior in larval zebrafish. *J Neurophysiol* **116**, 2067-2080.

Schweitzer, J., Gimnopoulos, D., Lieberoth, B.C., Pogoda, H.M., Feldner, J., Ebert, A., Schachner, M., Becker, T. & Becker, C.G. (2007) Contactin1a expression is associated

with oligodendrocyte differentiation and axonal regeneration in the central nervous system of zebrafish. *Molecular and Cellular Neurosciences* **35**, 194-207.

Sengupta, M. & Thirumalai, V. (2015) AMPA receptor mediated synaptic excitation drives state-dependent bursting in Purkinje neurons of zebrafish larvae. *Elife* **4**.

Shimoda, Y. & Watanabe, K. (2009) Contactins: emerging key roles in the development and function of the nervous system. *Cell Adhesion & Migration* **3**, 64-70.

Stoeckli, E.T. (2010) Neural circuit formation in the cerebellum is controlled by cell adhesion molecules of the Contactin family. *Cell Adhesion & Migration* **4**, 523-526.

Tanabe, K., Kani, S., Shimizu, T., Bae, Y.K., Abe, T. & Hibi, M. (2010) Atypical protein kinase C regulates primary dendrite specification of cerebellar Purkinje cells by localizing Golgi apparatus. *The Journal of Neuroscience: the official journal of the Society for Neuroscience* **30**, 16983-16992.

Thiele, T.R., Donovan, J.C. & Baier, H. (2014) Descending control of swim posture by a midbrain nucleus in zebrafish. *Neuron* **83**, 679-691.

Tomita, H. (1975) Mutant genes in the medaka. In: *Medaka (Kilifish)-Biology and Strains* (ed. T. Yamamoto), pp. 251-272. Keigaku Publishing Company, Tokyo.

Tomita, H. (1990) Strains and mutants of the medaka. In: *The Medaka Biology* (eds. E. Egami, K. Yamagami & S. Shima), pp. 111-128. The Tokyo University Press.

Tomita, H. (1992) The lists of the mutants and strains of the medaka, common gambusia, silver crucian carp, goldfish and golden venus fish maintained in the Laboratory of Freshwater Fish Stocks, Nagoya University. *Fish Biol J MEDAKA* **4**, 45-47.

Uematsu, K., Baba, Y., Kake, Y., Ikenaga, T., Moon, S.J., Miyai, Y. & Yoshida, M. (2007) Central mechanisms underlying fish swimming. *Brain Behav Evol* **69**, 142-150.

Virgintino, D., Ambrosini, M., D'Errico, P., Bertossi, M., Papadaki, C., Karagogeos, D. & Gennarini, G. (1999) Regional distribution and cell type-specific expression of the mouse F3 axonal glycoprotein: a developmental study. *The Journal of Comparative Neurology* **413**, 357-372.

Volkmann, K., Rieger, S., Babaryka, A. & Koster, R.W. (2008) The zebrafish cerebellar rhombic lip is spatially patterned in producing granule cell populations of different functional compartments. *Developmental Biology* **313**, 167-180.

Whitfield, T.T., Granato, M., van Eeden, F.J., Schach, U., Brand, M., Furutani-Seiki, M., Haffter, P., Hammerschmidt, M., Heisenberg, C.P., Jiang, Y.J., Kane, D.A., Kelsh, R.N., Mullins, M.C., Odenthal, J. & Nusslein-Volhard, C. (1996) Mutations affecting

development of the zebrafish inner ear and lateral line. *Development* **123**, 241-254.
Xenaki, D., Martin, I.B., Yoshida, L., Ohyama, K., Gennarini, G., Grumet, M., Sakurai, T. & Furley, A.J. (2011) F3/contactin and TAG1 play antagonistic roles in the regulation of sonic hedgehog-induced cerebellar granule neuron progenitor proliferation. *Development* **138**, 519-529.
Zee, D.S., Yamazaki, A., Butler, P.H. & Gucer, G. (1981) Effects of ablation of flocculus and paraflocculus of eye movements in primate. *J Neurophysiol* **46**, 878-899.

Table 1. Abnormal swimming behavior in medaka *cntn1b* mutants.

Mutant alleles	Normal (No. fish)			Abnormal (No. fish)			Abnormal ratio (%)
	Male	Female	Total	Male	Female	Total	
cntn1b$^{E3+35/+}$	9	6	15	0	0	0	0
cntn1b$^{E3+35/E3+35}$	0	0	0	3	3	6	100
cntn1b$^{E6-22/+}$	12	12	24	0	0	0	0
cntn1b$^{E6-22/E6-22}$	0	0	0	6	7	13	100
cntn1b$^{E6-4/+}$	19	9	28	0	0	0	0
cntn1b$^{E6-4/E6-4}$	0	0	0	7	3	10	100
ro/ro (*cntn1b*$^{ro/ro}$)	0	0	0	13	11	24	100
ro/cntn1b^{E3+35} (*cntn1b*$^{ro/E3+35}$)	0	0	0	17	15	32	100
ro/+ (*cntn1b*$^{ro/+}$)	25	11	36	0	0	0	0

Adult medaka fish (older than 3 months) with wild-type and/or mutant *cntn1b* genes were observed while swimming at normal breeding temperature (26 °C), and the percentage of fish with abnormal swimming behaviors (wobbling or rolling) was calculated for each type: *ro/ro* (*cntn1b*$^{ro/ro}$), *ro*-mutant homozygotes; *ro/cntn1b*$^{E3+35}$ (*cntn1b*$^{ro/E3+35}$), trans-heterozygotes of *ro* and *cntn1b*$^{E3+35}$ mutants; *ro/+* (*cntn1b*$^{ro/+}$), *ro*-mutant heterozygotes. All homozygous *cntn1b*$^{E3+35}$, *cntn1b*$^{E6-22}$, and *cntn1b*$^{E6-4}$ mutants showed abnormal swimming behaviors, while none of their heterozygous siblings did (*cntn1b*$^{E3+35}$, $p<0.0001$; *cntn1b*$^{E6-22}$, $p<0.0001$; *cntn1b*$^{E6-4}$, $p<0.0001$; Fisher's exact test). All homozygous *ro* mutants and all trans-heterozygous *cntn1b*$^{ro/E3+35}$ mutants also showed abnormal swimming behaviors, while none of the heterozygous *ro* mutant fish did. The difference between heterozygous and homozygous (trans-heterozygous) mutants was significant (*cntn1b*$^{ro/ro}$ vs. *cntn1b*$^{ro/+}$, $p<0.0001$; *cntn1b*$^{ro/E3+35}$ vs. *cntn1b*$^{ro/+}$, $p<0.0001$; Fisher's exact test).

Table 2. Abnormal swimming behavior in zebrafish *cntn1b* mutants.

Allele	Normal (No. fish)			Abnormal (No. fish)			Abnormal Ratio (%)
	Male	Female	Total	Male	Female	Total	
cntn1b$^{+/+}$	1	2	3	0	0	0	0
cntn1b$^{nub11/+}$	3	3	6	0	0	0	0
cntn1b$^{nub11/nub11}$	0	0	0	4	2	6	100

Adult sibling zebrafish (older than 3 months) with wild-type or mutant *cntn1b* were observed when swimming at normal breeding temperature (28 °C), and the percentage of fish with abnormal swimming behavior was calculated for wild-type (*cntn1b*$^{+/+}$), heterozygous (*cntn1b*$^{nub11/+}$), and homozygous (*cntn1b*$^{nub11/nub11}$) fish. All of the homozygous *cntn1b* mutants exhibited abnormal swimming behaviors, but none of the heterozygous or wild-type fish did; this difference was significant (wild-type vs. homozygous fish $p<0.05$; heterozygous vs. homozygous fish $p<0.01$; Fisher's exact test).

Figure legends

Figure 1. Linkage mapping of the medaka *ro* locus.

(A) The *ro* locus was mapped to chromosome 23. Polymorphic markers (Table S1) and the number of recombinations in the mutant genome are indicated. (B) The deletion in exon 15 of *cntn1b* in the *ro*-mutant genome. (C) PCR detection of exon 15 of *cntn1b* in wild-type (WT) and *ro*-mutant medaka (n=3 each). (D) RT-PCR showing *slc25a3b* (solute carrier family 25, member 3b), *ldhba* (lactose dehydrogenase Ba), *cntn1b*, and *ef1α* (elongation factor 1 alpha) expression in the brain (forebrain, midbrain, and hindbrain) from two WT and three *ro*-mutant adult fish. (E–F) Schematic representations of (E) the WT and *ro*-mutant Cntn1b proteins, (F) the medaka *cntn1b* gene structure and CRISPR/Cas9 targets, and (G) the WT and CRISPR *cntn1b* mutant proteins.

Figure 2. Expression of *cntn1a* and *cntn1b* in medaka embryos.

(A) RT-PCR detection of *cntn1a* and *cntn1b* expression in medaka embryos and larvae; *ef1α* was used as a loading control. (B–M) Expression of *cntn1a* and *cntn1b* at the pharyngula stage (stage 34), detected by whole-mount *in situ* hybridization. Views are dorsal with anterior to the left in (B–D, H–J), and the focus is adjusted to relatively ventral (B, H) or dorsal (C, I) levels. Views are lateral in (E–G, K–M), with dorsal up and anterior to the left. The focus is adjusted to lateral (E, K) or medial (F, L) levels. Scale bars: 200 μm in B (applies to B, C, E, F, H, I, K, and L) and 200 μm in D (applies to D, G, J, and M). Abbreviations: al, anterior lateral-line ganglion; nucmlf, nucleus of

the medial longitudinal fasciculus; pl, posterior lateral-line ganglion; RS, reticulospinal neurons; TeO, optic tectum; tg, trigeminal ganglion.

Figure 3. Expression of *cntn1a* and *cntn1b* in the medaka adult brain.

In situ hybridization of sagittal sections, showing the expression of (A, A′) *cntn1a*, (B, B′) *cntn1b*, (C), the Purkinje-cell marker aldolase Ca (*aldoca*), and (D) the granule-cell marker GABA A receptor, alpha 6b (*gabra6b*). (A′, B′) Higher-magnification views of the region of the cerebellum indicated in (A, B). Note that both *cntn1a* and *cntn1b* are expressed in Purkinje cells and granule cells. Scale bars: 1000 μm in A (applied to A, B) and 200 μm in A′ (applied to A′, B′, C, and D). Cb, cerebellum; Di, diencephalon; GCL, granule-cell layer; Hb, hindbrain; Hypo, hypothalamus; LCa, lobus caudalis cerebelli; ML, molecular layer; PCL, Purkinje-cell layer; Tel, telencephalon; TeO, optic tectum; TL, torus longitudinalis.

Figure 4. Medaka *ro* (*cntn1b*) mutants have relatively normal brain structure.

(A–D) Nissl staining of sagittal sections of adult wild-type (WT) and *ro*-mutant brains. Rectangles in (A, C) indicate the cerebellum; magnified views are shown in (B, D). (E–J) Sagittal sections showing the cerebellar region in the (E–G) WT and (H–J) *ro*-mutant brain, immunostained with antibodies against carbonic anhydrase 8 (Ca8), which marks Purkinje cells (green in E, G, H, and J), and against Vglut1, which marks granule-cell axons (magenta in F, G, I, and J). There were no apparent abnormalities in Purkinje cells or granule-cell axons in the adult cerebellum of the *ro*-mutant (n=4) compared to

the WT medaka (n=4). Scale bars: 1000 μm in A (applied to A, C), 200 μm in B (applied to B, D), and 200 μm in E (applied to E–J). Abbreviations are as in Figure 3.

Figure 5. Zebrafish *cntn1a* and *cntn1b* mutants.

Schematic representations of (A) the genomic structure of zebrafish *cntn1a* and *cntn1b*, indicating TALENs targets, and (B) wild-type (WT) and mutant Cntn1a and Cntn1b proteins. (C–Q) Sagittal sections of brains from (C–G) WT, (H–L) *cntn1a*-mutant, and (M–Q) *cntn1b*-mutant zebrafish, immunostained with antibodies against parvalbumin7 (Pvalb7), which marks Purkinje cells (green in C, E, F, H, J, K, M, O, and P) and against Vglut1, which marks granule-cell axons (magenta in D, E, G, I, J, L, N, O, and Q). Magnified views of the outlined regions in the top two rows are shown in the last two rows. Anterior is left; dorsal is up. There was no apparent abnormality in the Purkinje cells or granule-cell axons in the cerebellum of *cntn1b* mutants (n=3) compared to WT zebrafish (n=3). Scale bars: 200 μm in C (applied to C–E), H (applied to H–J), and M (applied to M–O), and 20 μm in F (applied to F, G), K (applied to K, L), and P (applied to P, Q).

Figure 6. Cntn1a and Cntn1b are not required for the formation of cerebellar neural circuits in early-stage zebrafish larvae.

Brains of (A–C) 5-dpf wild-type (WT) larvae, and (D–F) $cntn1a^{nub9/nub9}$, (G–I) $cntn1b^{nub11/nub11}$, and (J–L) $cntn1a^{nub9/nub9}$; $cntn1b^{nub11/nub11}$ mutant zebrafish larvae were immunostained with antibodies against parvalbumin7 (Pvalb7), which stains Purkinje

cells (green in A, C, D, F, G, I, J, and L) and against Vglut1, which marks granule-cell axons (magenta in B, C, E, F, H, I, K, and L). There were no apparent abnormalities in Purkinje cells or granule-cell axons in *cntn1a*$^{nub9/nub9}$ (n=6), *cntn1b*$^{nub11/nub11}$ (n=10), or *cntn1a*$^{nub9/nub9}$; *cntn1b*$^{nub11/nub11}$ (n=9) larvae compared to WT larvae (n=17). Scale bars: 50 μm in A (applied to A–C), D (applied to D–F), G (applied to G–I), and J (applied to J–L).

Figure 7. Cntn1b is required for optokinetic response (OKR) adaptation.

OKR adaptation in medaka was examined by horizontal oculomotor neural integrator (ONI) training. (A) Experimental setup. A camera takes magnified images around the animal's head at 60 frames/s (fs). The images are sent to a PC to detect rotation angles of the right eye in real time using a custom-made program running on LabVIEW. (B) The visual stimulus and an example of an eye-position trace during ONI instability training, in which random white dots were rotated away from the null position of the eye (dotted line) after each saccade. The direction and velocity of the rotation depend on the saccade landing position. For example, if the saccade is toward the nasal region of the orbit (positive eye position in the trace), the visual pattern rotates further toward the nasal direction. The further the landing position of the saccade from the null eye position, the faster the rotation speed, resulting in eye-position drifts as exemplified in the trace. Regression lines (magenta) were fitted to each eye-position drift to quantify how well the animal followed visual stimuli. (C) The mean learning curves of WT (gray circles, n=10) and *ro* (orange squares, n=10) fish, showing changes in the slope of the

regression lines fitted to eye-position drift during the ONI instability training. Error bars: standard error. Medaka *ro*-mutant fish showed defective learning in ONI training (p<0.05 by two-way repeated-measures ANOVA). AD/DA, AD/DA converter.

Figure 8. Cntn1b is required for controlling head position in rheotaxis.

(A) Experimental setup for analyzing swimming behavior. An adult medaka fish was placed into a swim-mill chamber and the water flow was set to a velocity of 1, 2, 3, or 4 body lengths (BL)/s. The movements of the fish were recorded with a video camera. The head movements were tracked, and the y-axis movement (the direction perpendicular to the water flow) was plotted. The graph shows data from a representative wild-type (WT) medaka fish. (B) Medaka *cntn1b* (*ro*) mutants cannot keep a stereotaxic position while swimming into the water flow. The y-axis head movements were separated into low-frequency (1–4 Hz, stereotaxic change) and high-frequency (4–20 Hz, yawing) movements using Lab Chart software, and the root mean square (RMS) was determined for each component. Figure S4 shows velocity-dependent changes in the RMS (1–4 BL/s). The graphs here show the RMS for WT (gray circles, n=13) and *ro*-mutant (orange squares, n=11) medaka in a water-flow velocity of 4 BL/s. Head positioning during swimming was significantly affected in the *ro*-mutant compared to WT fish (**p<0.001, ***p<0.0001, Welch's t test).

Supporting information

Supporting tables

Table S1. Markers for bulked segregant analysis.

Marker position	Marker types	Oligo 1	Oligo 2
3.65 Mb	SSLP	TAGTTTCATCATTGAAGGAAGCTCC	AAGGTCAACAAACGAGCTGG
3.71 Mb	SSLP	CCTTTGAGGGGACACAGGGT	CGGCTGTAACGCGGAAGGAT
3.75 Mb	RFLP(*EcoR*V)	GCAAGTTGAATTTTCATTGC	GGCAATGAGCTGTCAATCAA
3.78 Mb	RFLP(*Alu*I)	TCCTGGATCTGGATCTTCAAC	GTCCCTCCAATTCATCCTCA
3.82 Mb	SSLP	GTGGAAAAAGTGTGAAAAGTTGTGG	CGTATACGGTGCCCATATCA
3.90 Mb	SSLP	CAGGCTGTGGTTGTCGTCCT	CCTCAAGTGATTCCCAGGAG
3.92 Mb	SSLP	CCCCACTAGTTTCTACTTTGAGTC	AAAACCGATGTGCGCCTAAG
5.04 Mb	RFLP(*BstE*II)	CTATTGCACCTCCGAAGACTT	CGTCAGAATTAGCCGATTCA

Marker position: the distance between the marker and the telomere of chromosome 23. Genetic marker types: Simple Sequence Length Polymorphism (SSLP) or Amplified Fragment Length Polymorphism (AFLP, with polymorphic restriction-enzyme sites). Oligo 1 and 2: the PCR primer sequences used.

Table S2. PCR primers for generating medaka probes.

Gene symbol	Product	Forward primer	Reverse primer
cntn1a	Contactin1a	ATTGAGGGCAACTTGGTTATC	GCTCCACCCATTCAGGATAA
cntn1b	Contactin1b	CGGAATTCGTCTAAACTCAACGTG CTGTC	CCGCTCGAGTGCTTCCCACTTTGGGC GGGG
aldoca	Aldolase C, fructose-bisphosphate	AGCATGACGCTCCAGTTTCC	AATGCCATGCTGGTCCTGCT
gabra6b	GABA A receptor, alpha 6b	GGTGTAGAGGATTGTTCCGTTC	GTGCTGGACTGGCGTGATAA

The PCR primers used to isolate cDNA fragments are shown; the restriction-enzyme sites used for subcloning are underlined.

Supporting figures

Fig. S1. Medaka *cntn1b* mutants generated by the CRISPR/Cas9 system.

(A) Sequence comparison of the wild-type (WT) allele and the *cntn1b*$^{E3+35}$, *cntn1b*$^{E6-22}$, and *cntn1b*$^{E6-4}$ mutants. (B) Genotyping of WT and *cntn1b* CRISPR mutants. Genomic DNA was isolated from the tail fins of adult medaka fish and amplified by PCR. The PCR products were analyzed on agarose (left panel) or acrylamide (right panel) gels.

Fig. S2. Expression of *cntn1b* in adult medaka fish.

RT-PCR detection of *cntn1b* expression in heart, testis, intestine, liver, eye, and brain in adult medaka fish. *ef1α* was used as a loading control.

Fig. S3. Zebrafish *cntn1a* and *cntn1b* mutants generated by TALENs.

(A) Sequence comparison of the wild-type (WT) allele and the *cntn1a*^{nub8}, *cntn1a*^{nub9}, *cntn1b*^{nub10}, and *cntn1b*^{nub11} mutants. (B) For genotyping, genomic DNA was isolated from the fins of adult zebrafish and amplified by PCR. The PCR products were analyzed on acrylamide gels.

Fig. S4. Head positioning of wild-type and *ro* mutants at 1–4 BL/s.

Rheotaxis in adult wild-type (WT, gray circles, *n*=3) and *ro*-mutant medaka (orange squares, n=3) was analyzed as in Figure 8. The root mean square (RMS) of the low-frequency (1–4 Hz, body displacement) and high-frequency (4–20 Hz, head

yawing) head movement, determined with the fish swimming against water flow with a velocity of 1–4 body lengths (BL)/s, was plotted. Head positioning differed significantly between the WT and *ro*-mutant fish (1–4 Hz, $p<0.05$; 4–20 Hz, $p<0.05$; two-way repeated-measures ANOVA); $^{**}p<0.01$; $^{***}p<0.001$ (Bonferroni's post-hoc tests).

Fig. S5. Granule cells are not affected in zebrafish *cntn1a*, *cntn1b*, and *cntn1a/1b* mutant larvae.

Immunostaining of 5-dpf wild-type (WT) larvae and *cntn1a*, *cntn1b*, and *cntn1a/1b* mutant larvae with an anti-Neurod1 antibody. The number of Neurod1^{+} nuclei were counted and plotted in the graph. There was no significant difference between WT and mutant larvae (one-way ANOVA, $p>0.05$).

Movies

Movie S1. Swimming behavior of wild-type and *ro*-mutant medaka fish at 30 °C.

Movie S2. Swimming behavior of wild-type and *ro*-mutant medaka fish at 26 °C.

Movie S3. Swimming behavior of wild-type and *cntn1b*-mutant zebrafish.

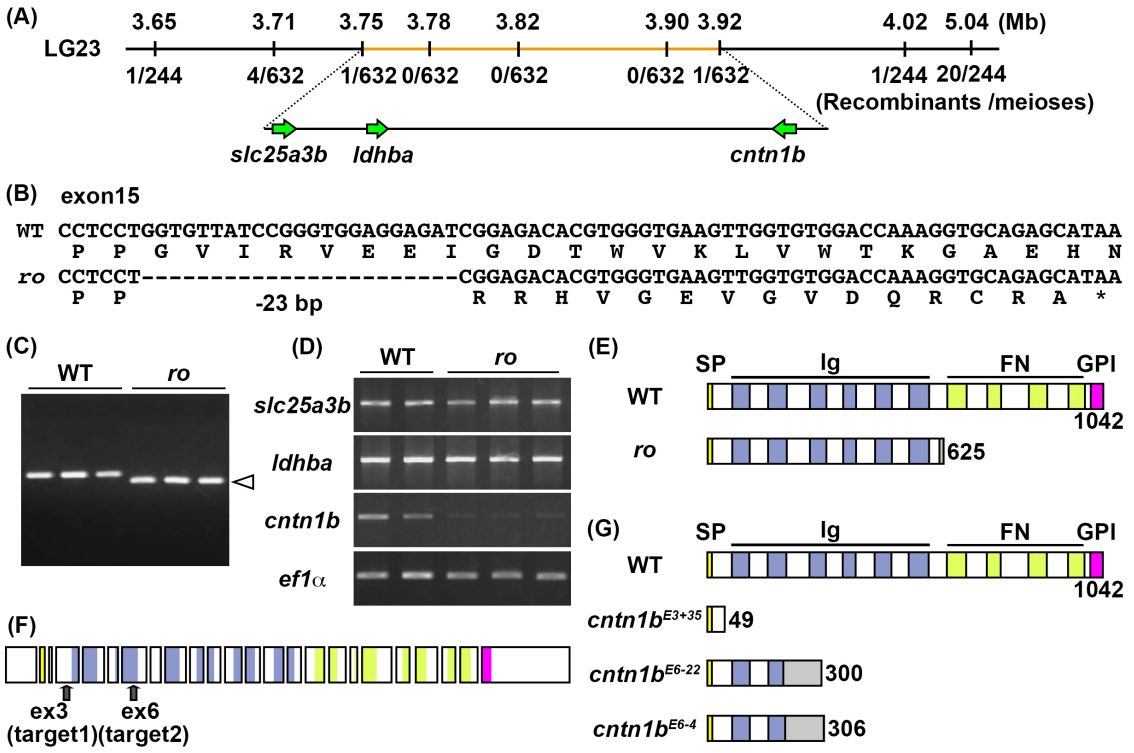

Figure 1. Linkage mapping of the medaka *ro* locus.
(A) The *ro* locus was mapped to chromosome 23. Polymorphic markers (Table S1) and the number of recombinations in the mutant genome are indicated. (B) The deletion in exon 15 of *cntn1b* in the *ro*-mutant genome. (C) PCR detection of exon 15 of *cntn1b* in wild-type (WT) and *ro*-mutant medaka (n=3 each). (D) RT-PCR showing *slc25a3b* (solute carrier family 25, member 3b), *ldhba* (lactose dehydrogenase Ba), *cntn1b*, and *ef1α* (elongation factor 1 alpha) expression in the brain (forebrain, midbrain, and hindbrain) from two WT and three *ro*-mutant adult fish. (E–F) Schematic representations of (E) the WT and *ro*-mutant Cntn1b proteins, (F) the medaka *cntn1b* gene structure and CRISPR/Cas9 targets, and (G) the WT and CRISPR *cntn1b* mutant proteins.

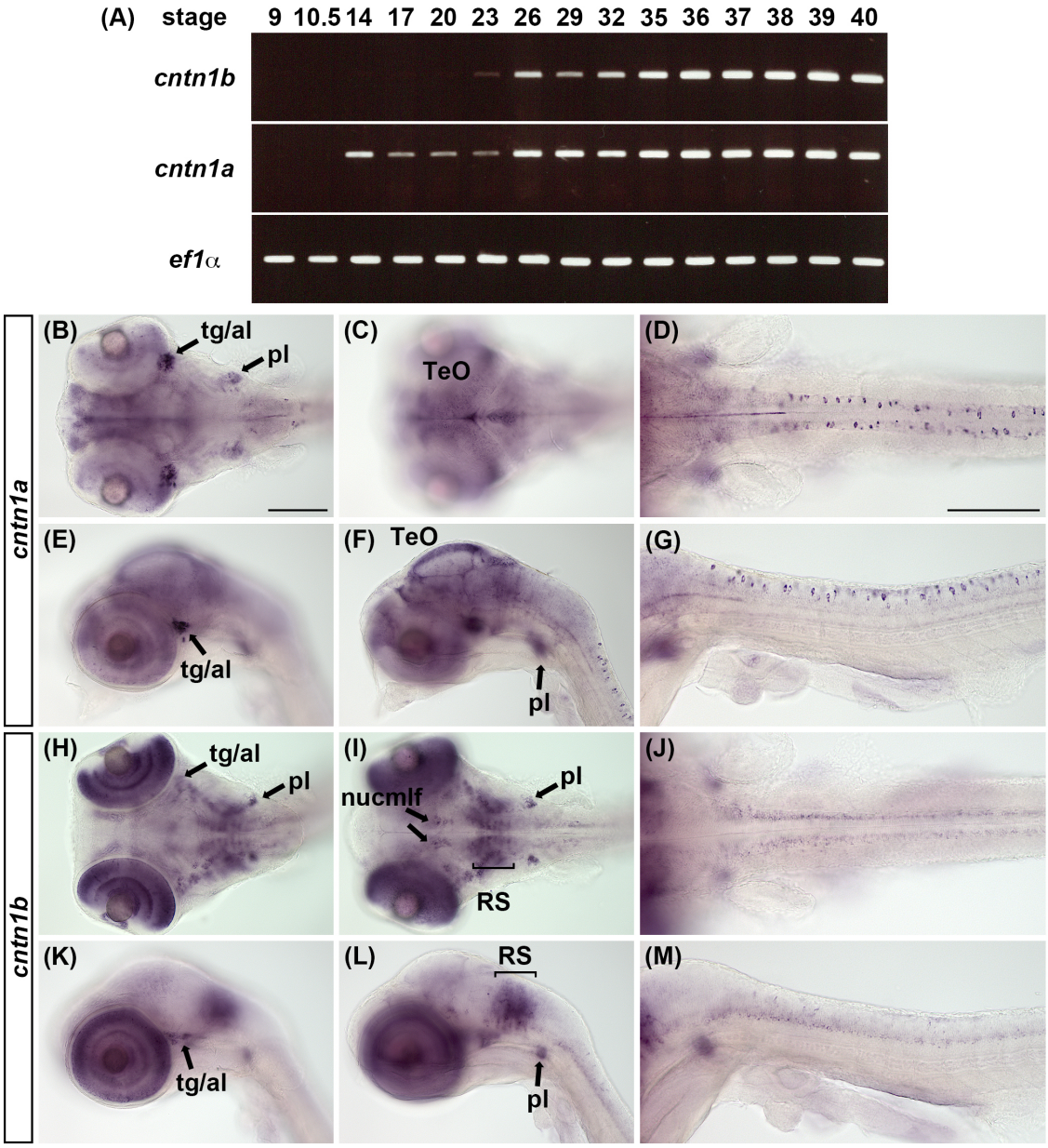

Figure 2. Expression of *cntn1a* and *cntn1b* in medaka embryos.
(A) RT-PCR detection of *cntn1a* and *cntn1b* expression in medaka embryos and larvae; *ef1α* was used as a loading control. (B–M) Expression of *cntn1a* and *cntn1b* at the pharyngula stage (stage 34), detected by whole-mount *in situ* hybridization. Views are dorsal with anterior to the left in (B–D, H–J), and the focus is adjusted to relatively ventral (B, H) or dorsal (C, I) levels. Views are lateral in (E–G, K–M), with dorsal up and anterior to the left. The focus is adjusted to lateral (E, K) or medial (F, L) levels. Scale bars: 200 μm in B (applies to B, C, E, F, H, I, K, and L) and 200 μm in D (applies to D, G, J, and M). Abbreviations: al, anterior lateral-line ganglion; nucmlf, nucleus of the medial longitudinal fasciculus; pl, posterior lateral-line ganglion; RS, reticulospinal neurons; TeO, optic tectum; tg, trigeminal ganglion.

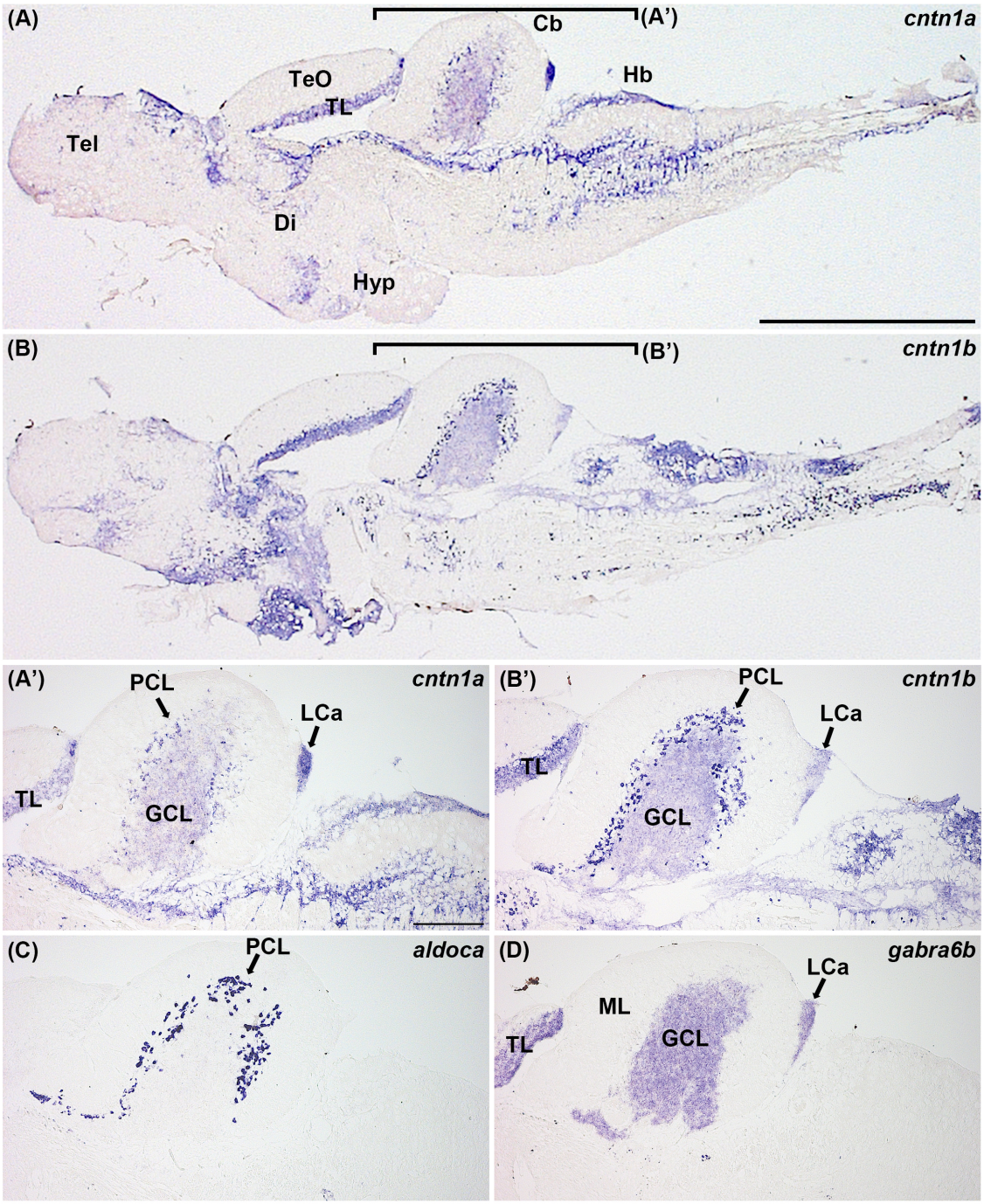

Figure 3. Expression of *cntn1a* and *cntn1b* in the medaka adult brain.
In situ hybridization of sagittal sections, showing the expression of (A, A′) *cntn1a*, (B, B′) *cntn1b*, (C), the Purkinje-cell marker aldolase Ca (*aldoca*), and (D) the granule-cell marker GABA A receptor, alpha 6b (*gabra6b*). (A′, B′) Higher-magnification views of the region of the cerebellum indicated in (A, B). Note that both *cntn1a* and *cntn1b* are expressed in Purkinje cells and granule cells. Scale bars: 1000 μm in A (applied to A, B) and 200 μm in A′ (applied to A′, B′, C, and D). Cb, cerebellum; Di, diencephalon; GCL, granule-cell layer; Hb, hindbrain; Hypo, hypothalamus; LCa, lobus caudalis cerebelli; ML, molecular layer; PCL, Purkinje-cell layer; Tel, telencephalon; TeO, optic tectum; TL, torus longitudinalis.

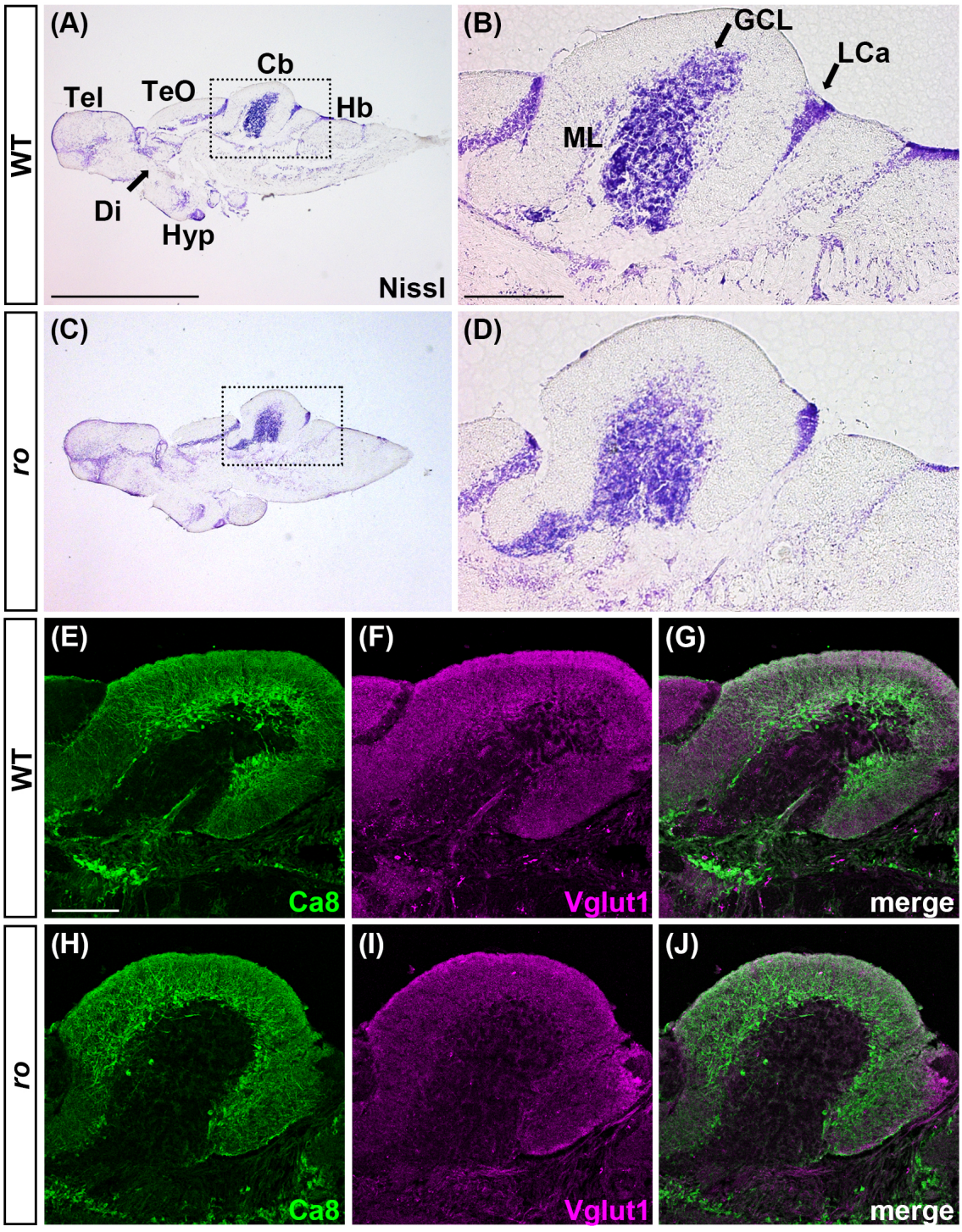

Figure 4. Medaka *ro* (*cntn1b*) mutants have relatively normal brain structure.
(A–D) Nissl staining of sagittal sections of adult wild-type (WT) and *ro*-mutant brains. Rectangles in (A, C) indicate the cerebellum; magnified views are shown in (B, D). (E–J) Sagittal sections showing the cerebellar region in the (E–G) WT and (H–J) *ro*-mutant brain, immunostained with antibodies against carbonic anhydrase 8 (Ca8), which marks Purkinje cells (green in E, G, H, and J), and against Vglut1, which marks granule-cell axons (magenta in F, G, I, and J). There were no apparent abnormalities in Purkinje cells or granule-cell axons in the

adult cerebellum of the *ro*-mutant (n=4) compared to the WT medaka (n=4). Scale bars: 1000 μm in A (applied to A, C), 200 μm in B (applied to B, D), and 200 μm in E (applied to E–J). Abbreviations are as in Figure 3.

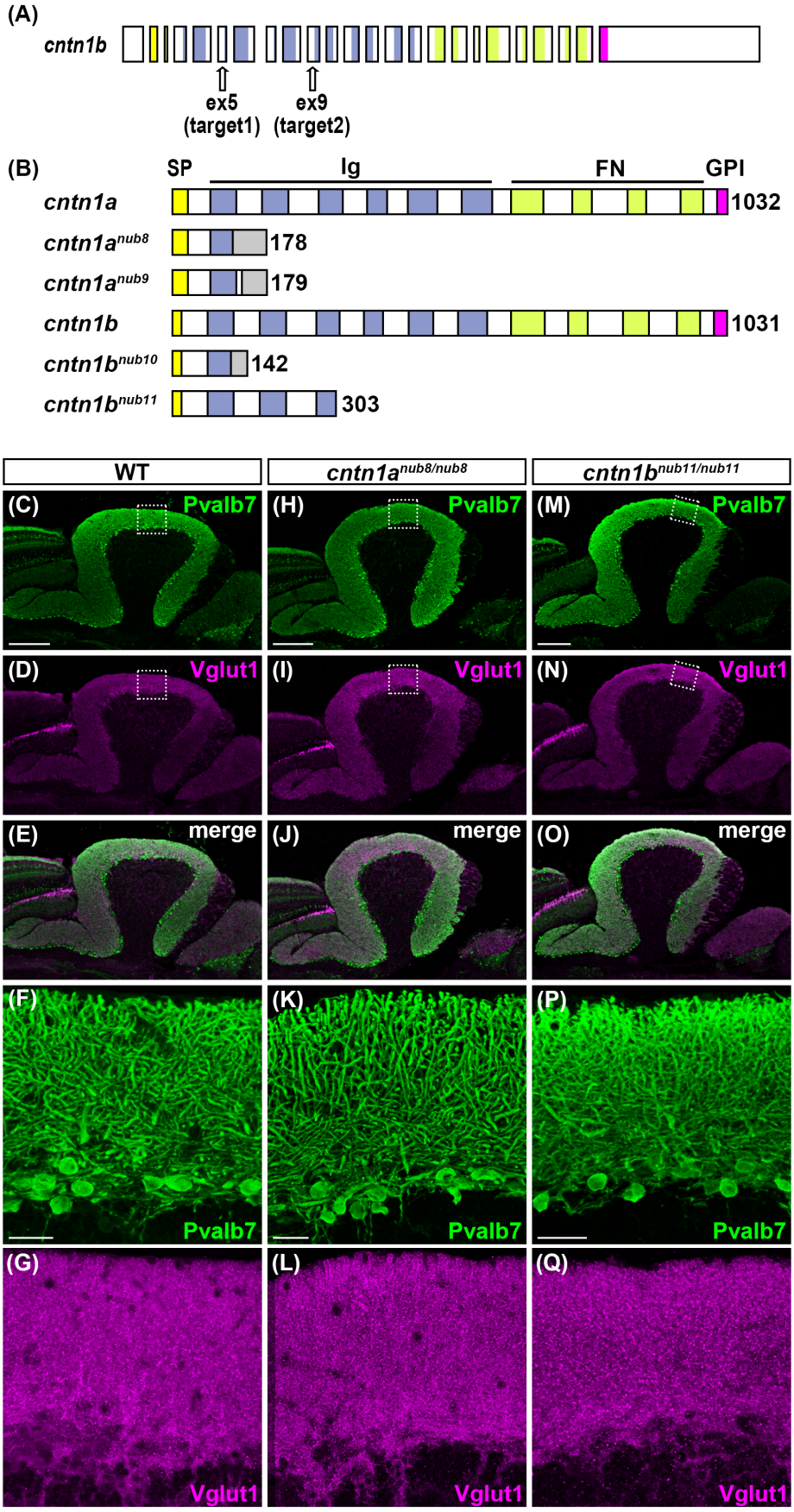
(A)
cntn1b
ex5
(target1)
ex9
(target2)
(B)
SP
Ig
FN
GPI
cntn1a
1032
cntn1a^nub8
178
cntn1a^nub9
179
cntn1b
1031
cntn1b^nub10
142
cntn1b^nub11
303
WT
cntn1a^nub8/nub8
cntn1b^nub11/nub11
(C)
Pvalb7
(H)
Pvalb7
(M)
Pvalb7
(D)
Vglut1
(I)
Vglut1
(N)
Vglut1
(E)
merge
(J)
merge
(O)
merge
(F)
Pvalb7
(K)
Pvalb7
(P)
Pvalb7
(G)
Vglut1
(L)
Vglut1
(Q)
Vglut1

Figure 5. Zebrafish *cntn1a* and *cntn1b* mutants.
Schematic representations of (A) the genomic structure of zebrafish *cntn1a* and *cntn1b*, indicating TALENs targets, and (B) wild-type (WT) and mutant Cntn1a and Cntn1b proteins. (C–Q) Sagittal sections of brains from (C–G) WT, (H–L) *cntn1a*-mutant, and (M–Q) *cntn1b*-mutant zebrafish, immunostained with antibodies against parvalbumin7 (Pvalb7), which marks Purkinje cells (green in C, E, F, H, J, K, M, O, and P) and against Vglut1, which marks granule-cell axons (magenta in D, E, G, I, J, L, N, O, and Q). Magnified views of the outlined regions in the top two rows are shown in the last two rows. Anterior is left; dorsal is up. There was no apparent abnormality in the Purkinje cells or granule-cell axons in the cerebellum of *cntn1b* mutants (n=3) compared to WT zebrafish (n=3). Scale bars: 200 μm in C (applied to C–E), H (applied to H–J), and M (applied to M–O), and 20 μm in F (applied to F, G), K (applied to K, L), and P (applied to P, Q).

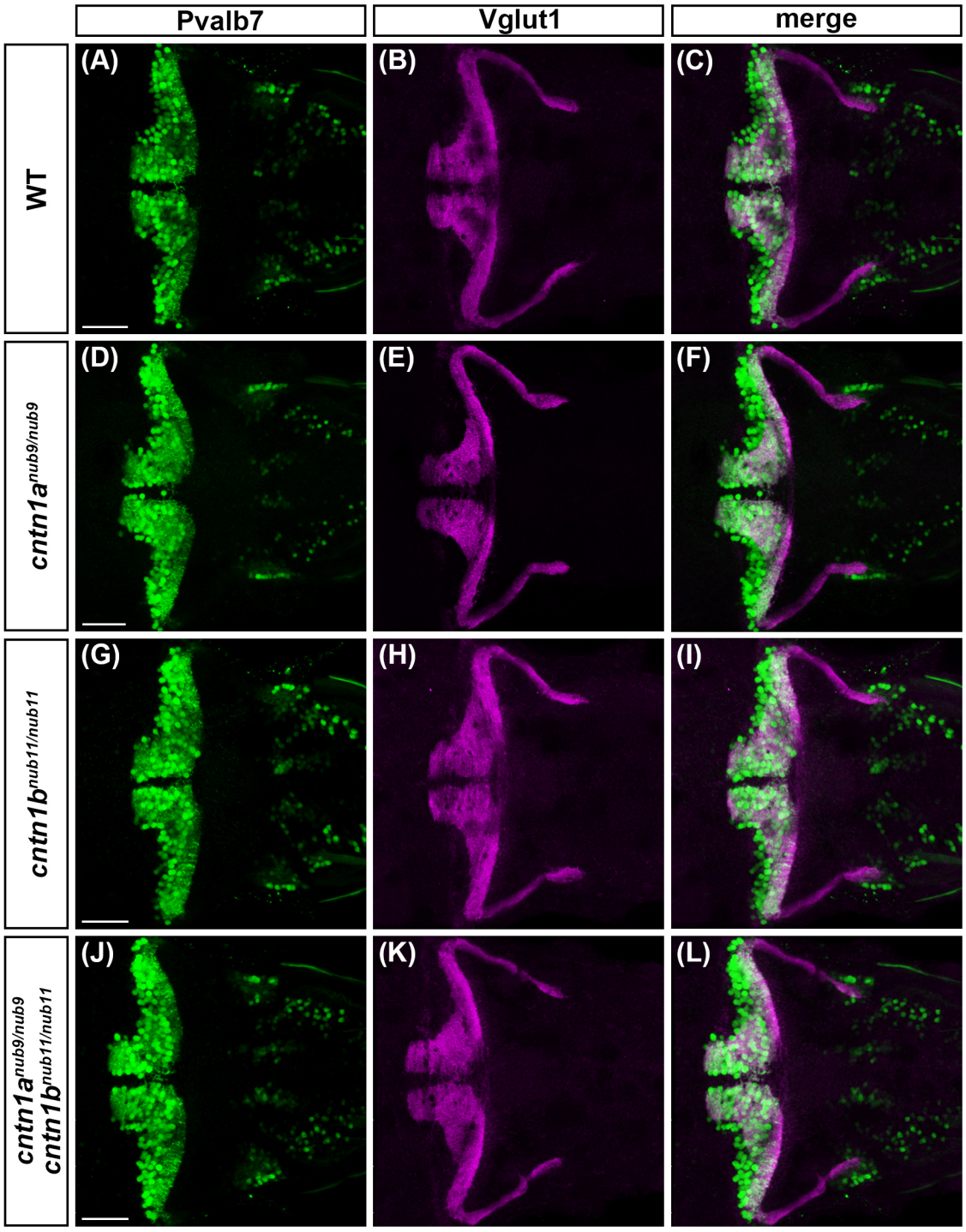

Figure 6. Cntn1a and Cntn1b are not required for the formation of cerebellar neural circuits in early-stage zebrafish larvae.

Brains of (A–C) 5-dpf wild-type (WT) larvae, and (D–F) *cntn1a*$^{nub9/nub9}$, (G–I) *cntn1b*$^{nub11/nub11}$, and (J–L) *cntn1a*$^{nub9/nub9}$*; cntn1b*$^{nub11/nub11}$ mutant zebrafish larvae were immunostained with antibodies against parvalbumin7 (Pvalb7), which stains Purkinje cells (green in A, C, D, F, G, I, J, and L) and against Vglut1, which marks granule-cell axons (magenta in B, C, E, F, H, I, K, and L). There were no apparent abnormalities in Purkinje cells or granule-cell axons in

cntn1a$^{nub9/nub9}$ (n=6), *cntn1b*$^{nub11/nub11}$ (n=10), or *cntn1a*$^{nub9/nub9}$; *cntn1b*$^{nub11/nub11}$ (n=9) larvae compared to WT larvae (n=17). Scale bars: 50 μm in A (applied to A–C), D (applied to D–F), G (applied to G–I), and J (applied to J–L).

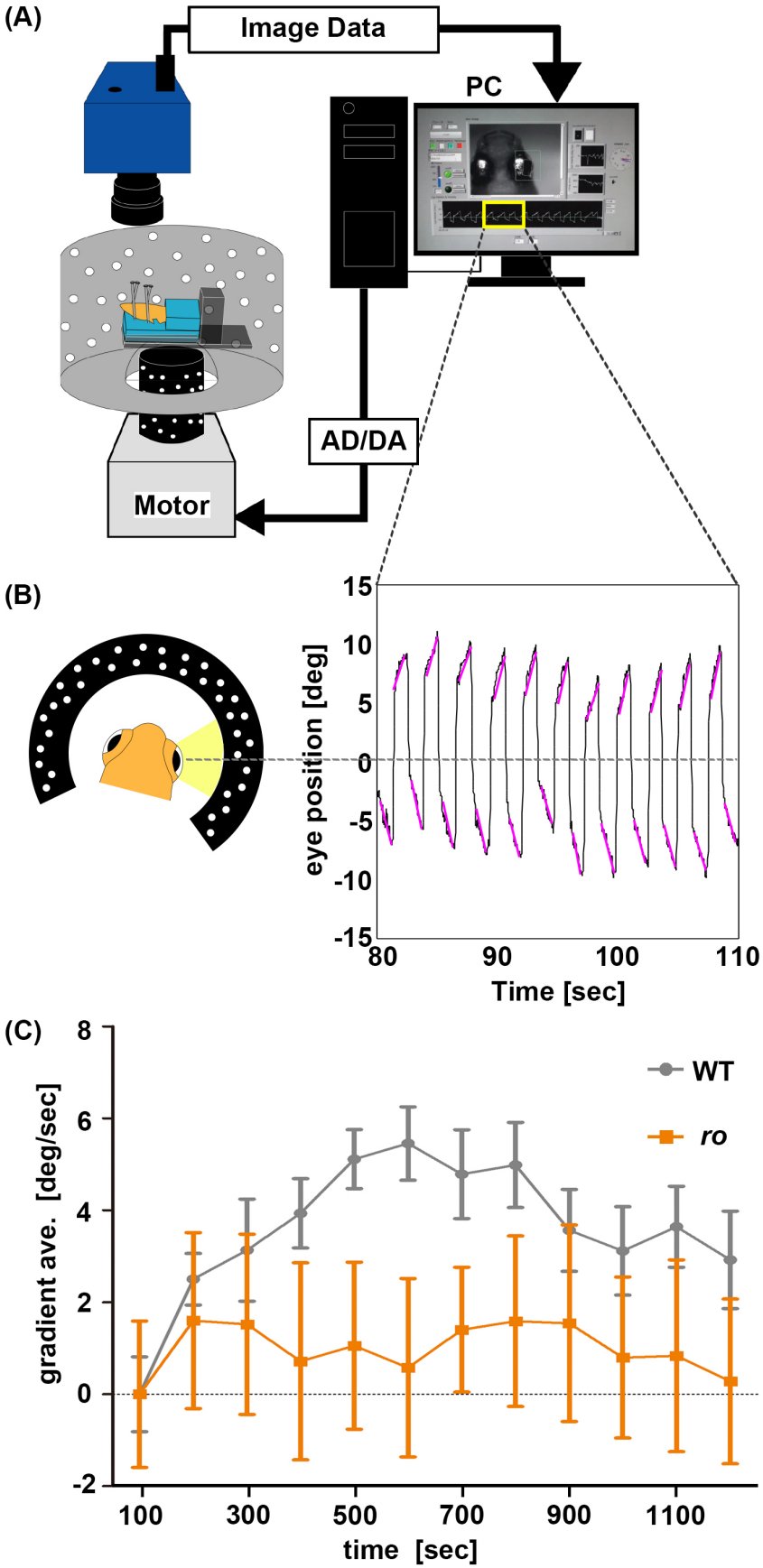
(A)
Image Data
PC
AD/DA
Motor
(B)
eye position [deg]
15
10
5
0
-5
-10
-15
80
90
100
110
Time [sec]
(C)
gradient ave. [deg/sec]
8
6
4
2
0
-2
100
300
500
700
900
1100
time [sec]
WT
ro

Figure 7. Cntn1b is required for optokinetic response (OKR) adaptation.
OKR adaptation in medaka was examined by horizontal oculomotor neural integrator (ONI) training. (A) Experimental setup. A camera takes magnified images around the animal's head at 60 frames/s (fs). The images are sent to a PC to detect rotation angles of the right eye in real time using a custom-made program running on LabVIEW. (B) The visual stimulus and an example of an eye-position trace during ONI instability training, in which random white dots were rotated away from the null position of the eye (dotted line) after each saccade. The direction and velocity of the rotation depend on the saccade landing position. For example, if the saccade is toward the nasal region of the orbit (positive eye position in the trace), the visual pattern rotates further toward the nasal direction. The further the landing position of the saccade from the null eye position, the faster the rotation speed, resulting in eye-position drifts as exemplified in the trace. Regression lines (magenta) were fitted to each eye-position drift to quantify how well the animal followed visual stimuli. (C) The mean learning curves of WT (gray circles, n=10) and *ro* (orange squares, n=10) fish, showing changes in the slope of the regression lines fitted to eye-position drift during the ONI instability training. Error bars: standard error. Medaka *ro*-mutant fish showed defective learning in ONI training ($p<0.05$ by two-way repeated-measures ANOVA). AD/DA, AD/DA converter.

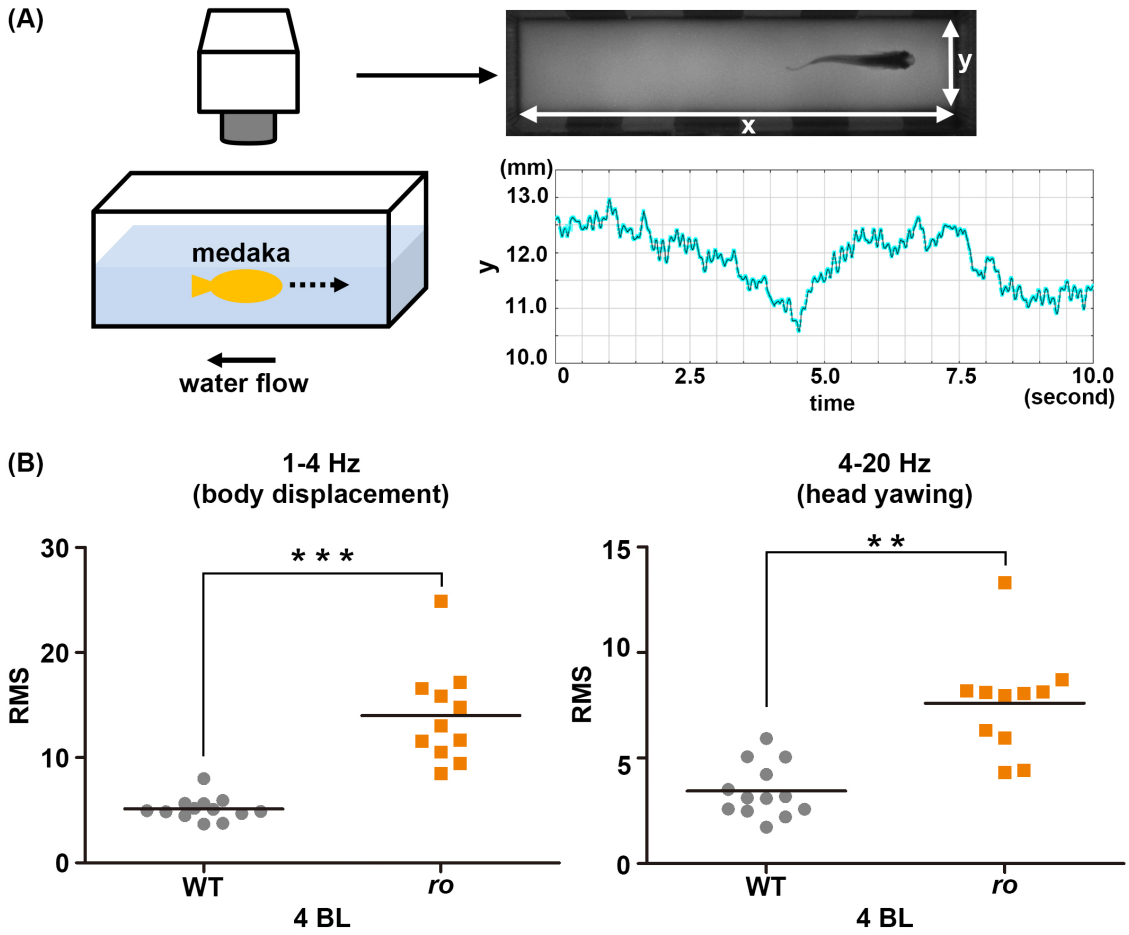

Figure 8. Cntn1b is required for controlling head position in rheotaxis.
(A) Experimental setup for analyzing swimming behavior. An adult medaka fish was placed into a swim-mill chamber and the water flow was set to a velocity of 1, 2, 3, or 4 body lengths (BL)/s. The movements of the fish were recorded with a video camera. The head movements were tracked, and the y-axis movement (the direction perpendicular to the water flow) was plotted. The graph shows data from a representative wild-type (WT) medaka fish. (B) Medaka *cntn1b* (*ro*) mutants cannot keep a stereotaxic position while swimming into the water flow. The y-axis head movements were separated into low-frequency (1–4 Hz, stereotaxic change) and high-frequency (4–20 Hz, yawing) movements using Lab Chart software, and the root mean square (RMS) was determined for each component. Figure S4 shows velocity-dependent changes in the RMS (1–4 BL/s). The graphs here show the RMS for WT (gray circles, n=13) and *ro*-mutant (orange squares, n=11) medaka in a water-flow velocity of 4 BL/s. Head positioning during swimming was significantly affected in the *ro*-mutant compared to WT fish (**p<0.001, ***p<0.0001, Welch's t test).

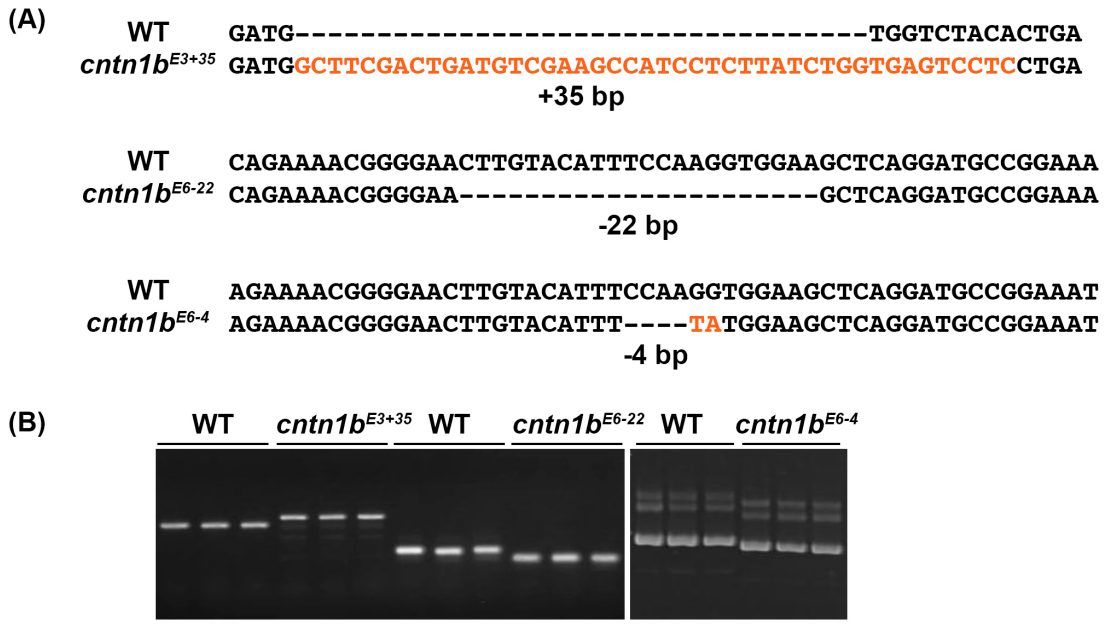

Fig. S1. Medaka *cntn1b* mutants generated by the CRISPR/Cas9 system.
(A) Sequence comparison of the wild-type (WT) allele and the *cntn1b*$^{E3+35}$, *cntn1b*$^{E6-22}$, and *cntn1b*$^{E6-4}$ mutants. (B) Genotyping of WT and *cntn1b* CRISPR mutants. Genomic DNA was isolated from the tail fins of adult medaka fish and amplified by PCR. The PCR products were analyzed on agarose (left panel) or acrylamide (right panel) gels.

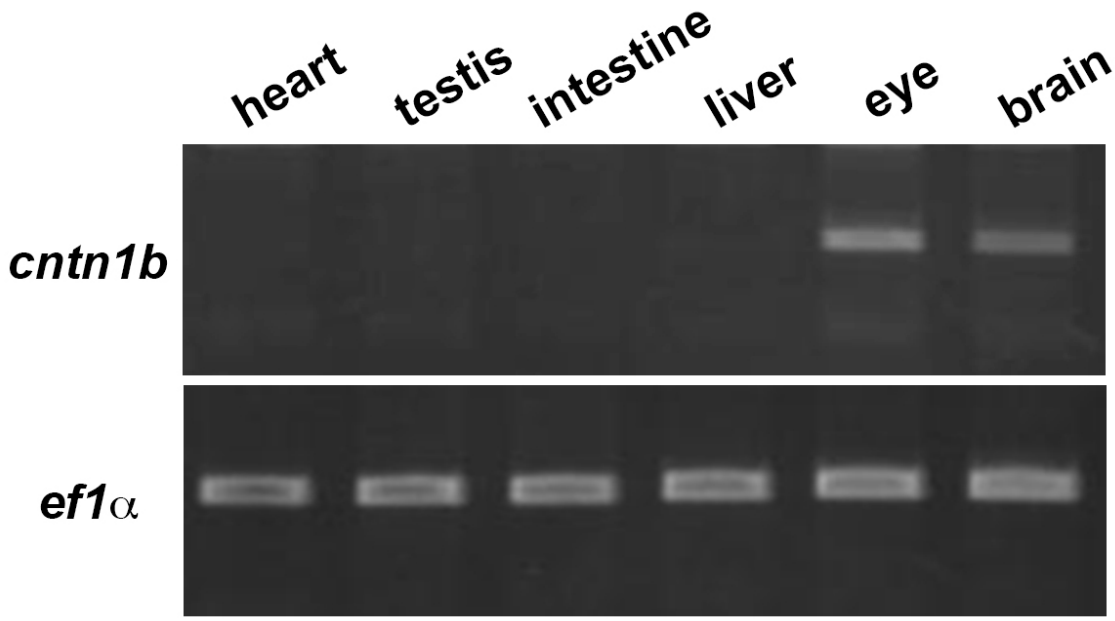

Fig. S2. Expression of *cntn1b* in adult medaka fish.
RT-PCR detection of *cntn1b* expression in heart, testis, intestine, liver, eye, and brain in adult medaka fish. *ef1α* was used as a loading control.

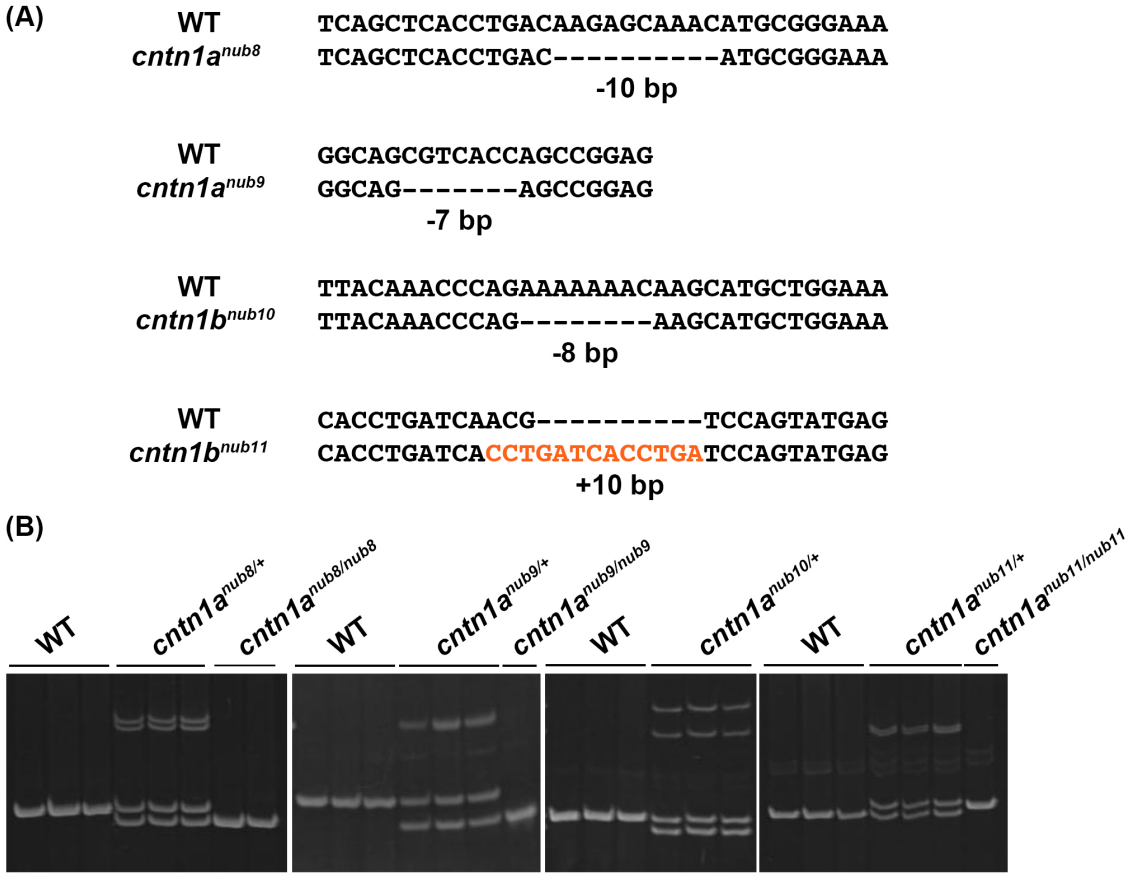

Fig. S3. Zebrafish *cntn1a* and *cntn1b* mutants generated by TALENs.
(A) Sequence comparison of the wild-type (WT) allele and the *cntn1a*^{nub8}, *cntn1a*^{nub9}, *cntn1b*^{nub10}, and *cntn1b*^{nub11} mutants. (B) For genotyping, genomic DNA was isolated from the fins of adult zebrafish and amplified by PCR. The PCR products were analyzed on acrylamide gels.

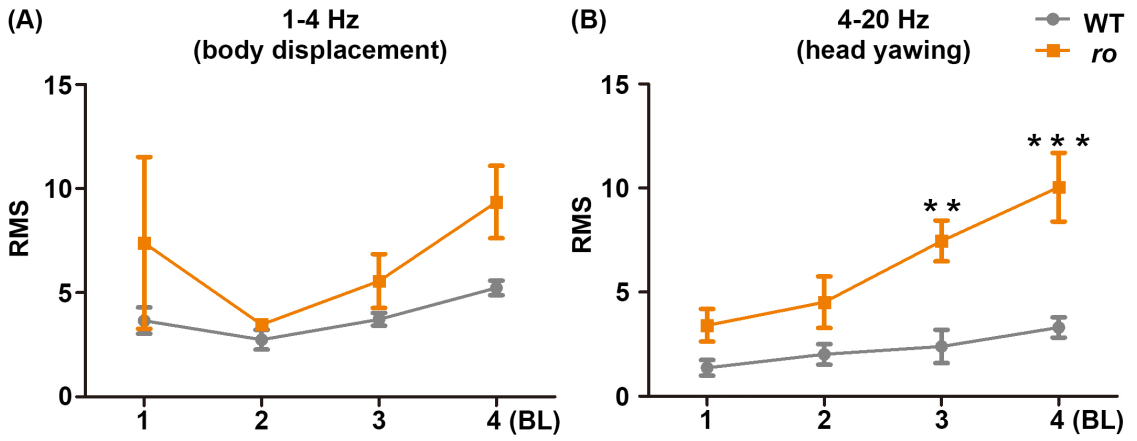

Fig. S4. Head positioning of wild-type and *ro* mutants at 1–4 BL/s.
Rheotaxis in adult wild-type (WT, gray circles, *n*=3) and *ro*-mutant medaka (orange squares, n=3) was analyzed as in Figure 8. The root mean square (RMS) of the low-frequency (1–4 Hz, body displacement) and high-frequency (4–20 Hz, head yawing) head movement, determined with the fish swimming against water flow with a velocity of 1–4 body lengths (BL)/s, was plotted. Head positioning differed significantly between the WT and *ro*-mutant fish (1–4 Hz, $p<0.05$; 4–20 Hz, $p<0.05$; two-way repeated-measures ANOVA); $^{**}p<0.01$; $^{***}p<0.001$ (Bonferroni's post-hoc tests).

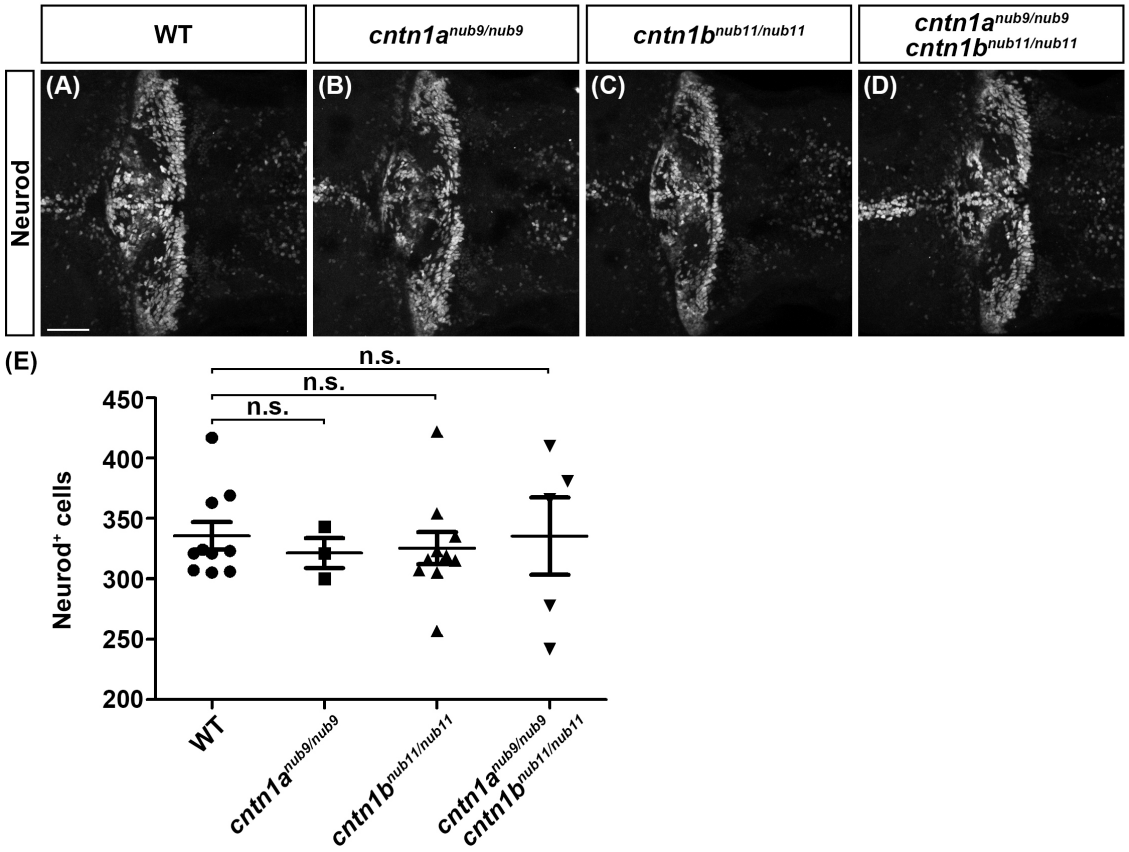

Fig. S5. Granule cells are not affected in zebrafish *cntn1a*, *cntn1b*, and *cntn1a/1b* mutant larvae. Immunostaining of 5-dpf wild-type (WT) larvae and *cntn1a*, *cntn1b*, and *cntn1a/1b* mutant larvae with an anti-Neurod1 antibody. The number of Neurod1^{+} nuclei were counted and plotted in the graph. There was no significant difference between WT and mutant larvae (one-way ANOVA, $p>0.05$).